NANOFLUIDICS IN TAILORED CARBON NANOTUBE MEMBRANES

By

SCOTT ALLAN MILLER

A DISSERTATION PRESENTED TO THE GRADUATE SCHOOL
OF THE UNIVERSITY OF FLORIDA IN PARTIAL FULFILLMENT
OF THE REQUIREMENTS FOR THE DEGREE OF
DOCTOR OF PHILOSOPHY

UNIVERSITY OF FLORIDA

2004

This dissertation is dedicated to my mother, Barbara R. Miller-Collins, whose persistence and resiliency amazes; and in memory of my father, Dr. Allan G. Miller, whose strength, dedication, and entrepreneurship showed me pathways that I never would have otherwise found.

ACKNOWLEDGEMENTS

I have been fortunate enough in my graduate studies to work with a disproportionate number of very fine people in the Martin Group. Professor Charles Martin has put together a quality research group and a strong research program which I am proud to have been associated with. He has continuously steered me into dynamic, fertile, and interesting areas of research and has enthusiastically lent his creativity and expertise towards solving whatever challenges might be encountered.

As a group, my co-workers have been generous with their support, help, and knowledge. As individuals, they have been friends, mentors, and guides in my development as a scientist and a person. I especially thank Sang Bok Lee and Mark Wirtz for great generosity of time and energy in support of my work. Kshama Jirage and Charlie Patrissi offered excellent advice and direction in my early studies. Fausto Croce, Katsumi Yamada, Punit Kohli, Fatih Buyukserin, and Zuzanna Siwy have engaged me in untold numbers of interesting, insightful, and beneficial technical discussions.

Time after time, Elizabeth Heins's tireless and thankless efforts have kept the group from succumbing to the entropic abyss and just plain made the lab a better place. I also must thank her for keeping extra paper under her desk. Q Trofin kept me supplied with beautiful alumina membranes, tasty coffee, and a forgiving personality for me to harass; for this I owe her the deepest gratitude. Erich Steinle and Butler Raines possessed the admirable qualities of generally being ready for lunch time and happy hour. Shufang Yu, Damian Odom, John Wharton, Rob Sides, and Chad Harrell have kept it real, making the

lab a fun and good place to be. Rahela Gasparac has been a constant source of professional perspective for myself and undoubtedly others. Dave Mitchell has been ubiquitous and extravagant in his technical support and temporal generosity. I thank him for many of the SEM images appearing in the text, extensive editing of written materials and oral presentations, sound technical advice, and for being a good friend.

Professor Vaneica Young has been very helpful and thorough in sharing her expertise in XPS analysis of many samples. I owe thanks to Dr. Viswanath Krishnamoorthy of MAIC and Fred Bennett of the Electron Microscopy Core Laboratory for excellent instruction and assistance in TEM and SEM analysis. Professor Henry White has made fruitful suggestions regarding investigations into electroosmotic flow. Professor Richard McCreery offered valuable insights into the chemistry of carbons.

On a personal level, Debbie Spivak and Howard Newman have been great friends and I will think of them often. May the German, Alina the Lithuanian, and Tom and Lynn Saunders have been great roommates and helped to make the last few months of my studies so enjoyable. Dog Lennon has been very good and is so considerate with his business. Thanks to J.J. Finley and UFUCT for many good memories. The distances are great but I owe special thanks to Stephan Paglieri, Eric LoPresti, Darien Heap, and Robi Sen for being good friends over the years, and they remain in my thoughts.

My family has been tireless and unconditional advocates throughout my graduate studies and I can't express what that has meant to me. I thank Chris Collins, Paul Williams and Bren Williams, and Burnie Miller for always believing in me. I would especially like to thank my mother, Barbara Miller-Collins for all of her love, support, and resiliency.

TABLE OF CONTENTS

Page

ACKNOWLEDGMENTS iii

LIST OF TABLES vii

LIST OF FIGURES viii

ABSTRACT x

CHAPTER

1 INTRODUCTION 1

Carbon Nanotubes 1
Synthesis of Carbon Nanotubes 2
Carbon Membranes 4
Template Synthesis 8
Gold Nanotube Membranes 9
Anodic Aluminum Oxide Template Membranes 10
Electroosmotic Flow 14
The Electric Double Layer 15
Electroosmotic Flow 16
Dynamic Electromodulation of Electroosmotic Flow 18
Chapter Summaries 19

2 SYNTHESIS AND TAILORING CARBON NANOTUBE MEMBRANES BY THE TEMPLATE METHOD 23

Introduction 23
Experimental 26
Materials 26
Preparation of Carbon Nanotube Membranes 26
Electron Microscopy 27
Results and Discussion 27
Template Synthesis of Carbon Nanotube Membranes 27
Effect of High CVD Rate on Carbon Nanotube Growth 30
Characterization of the CVD Template Method 31
Branched Carbon Nanotubes 33
Carbon Nanotube Membranes Prepared in Lab-Grown Alumina 34
Conclusions 39

3 ELECTROOSMOTIC FLOW IN TEMPLATE-PREPARED CARBON NANOTUBE MEMBRANES 39

Introduction 39
Experimental 40
Materials 40
Preparation of the Carbon Nanotube Membranes 41
X-Ray Photoelectron Spectroscopy (XPS) 41
Permeation Measurements 42
Electron Microscopy 43
Results and Discussion 45
Electron Microscopy 45
XPS 46
Effect of Magnitude of the Applied Current on Permeate (Phenol) Flux 47
Calculation of the Electroosmotic Velocity 49
Effect of Applied Current Density on υ_{eo} 51
Effect of Ionic Strength of the Electrolyte on υ_{eo} 53
Effect of Solution pH on υ_{eo} 56
The Effect of Cationic Surfactant on υ_{eo} 60
Conclusions 62

4 TAILORING ELECTROKINETIC PROPERTIES OF CARBON NANOTUBE MEMBRANE ELECTRODES 64

Introduction 64
Expermimental 67
Materials 67
Preparation of the Carbon Nanotube Membrane Electrodes 68
Electrochemical Derivatization of Carbon Nanotubes with Primary Amines 69
Growth of PPO Nanotubes Inside Carbon Nanotubes 70
Electromodification of CNMs with Poly(vinylferrocene) 70
Permeation and EOF Measurements 71
Results and Discussion 72
EOF in Carbon Nanotube Membranes 72
The Effect of Electrochemical Derivatization on υ_{eo} 73
EOF Passivation in CN/PPO Membranes 76
Redox-Modulated EOF in CN/PVFc Membranes 78
Conclusions 82

5 CONCLUSIONS 84

LIST OF REFERENCES 89

BIOGRAPHICAL SKETCH 99

LIST OF TABLES

Table Page

3-1: Effect of applied current density on the flux, enhancement factor and electroosmotic velocity in the carbon nanotube membrane 49

LIST OF FIGURES

Figure Page

1-1. Array of template-synthesized carbon nanotubes (scanning electron micrograph). . 5

1-2. Template synthesis of carbon nanotube membranes by CVD (schematic). 7

1-3. Commonly used nanoporous template membranes (SEM micrographs). 9

1-4. AAO membrane with asymmetric branched pores (illustration). 11

1-5. Porous anodic aluminum oxide film with barrier layer on aluminum anode (illustration). 12

1-6. A negatively charged pore and the resulting electric double layer in electrolyte solution (illustration). 17

2-1. 200-nm Anodisc™ template membrane (SEM micrograph). 28

2-2. Carbon nanotubes grown by CVD in 200-nm Anodisc™ template membrane (electron micrographs). 29

2-3. Carbon nanotube grown at a high CVD rate in 200-nm Anodisc™ template (TEM micrographs). 30

2-4. %Carbon vs. CVD time for carbon nanotube membranes synthesized at 730 °C. . 32

2-5. Average rate of carbon deposition vs. CVD temperature for carbon nanotube membranes. 33

2-6. Carbon nanotubes grown at a high CVD rate in 20-nm Anodisc™ membrane (electron micrographs). 34

2-7. Carbon nanotubes grown at 700 °C in a lab-grown AAO template (TEM micrographs). 35

2-8. Lab-grown double-anodization AAO membrane (SEM micrographs). 36

2-9. Carbon nanotubes grown in a home-grown double-anodization AAO membrane (electron micrographs). 37

3-1. CNM permeation cell setup schematics (illustrations). 43

3-2. High resolution C 1s XPS spectrum showing the experimental spectrum, the fitted envelope, and the individual peaks for the fit. 47

3-3. Micromoles of phenol transported vs. time at various values of applied current density. 48

3-4. Effect of applied current density on CNM transport phenomenon. 52

3-5. Plots of electroosmotic flow velocity vs. the ionic strength of the permeate and feed solutions..... 54

3-6. Effect of solution pH on EOF and CNM zeta potential. 57

3-7. Cationic surfactant bilayer method of dynamic electroosmotic flow reversal (illustration). 61

3-8. Reversal of EOF with cationic surfactant..... 61

4-1. Redox-modulated electroosmotic flow in a carbon nanotube membrane modified with ferrocene (illustration). 68

4-2. Plots of electroosmotic velocity vs. applied current density for derivatized CNMs.74

4-3. Electrochemical synthesis and characterization of CN/PPO membrane electrode (cyclyic votammograms). 77

4-4. Micromoles of phenol transported vs. time at various values of applied current density across a CN/PPO membrane..... 78

4-5. Cyclic voltammograms for the CNM and the CN/PVFc membranes. 79

4-6. Plots of electroosmotic flow velocity vs applied current density for totally oxidized (●) and totally reduced (♦) CN/PVFc membranes. 80

4-7. Effect of redox modulation on EOF and zeta potential of CN/PVFc membrane electrode. 81

Abstract of Dissertation Presented to the Graduate School
of the University of Florida in Partial Fulfillment of the
Requirements for the Degree of Doctor of Philosophy

NANOFLUIDICS IN TAILORED CARBON NANOTUBE MEMBRANES

Scott Allan Miller

May 2004

Chair: Professor Charles R. Martin
Major Department: Chemistry

Carbon nanotubes and carbon membranes are two rapidly growing areas of research. At the interface of these two areas are carbon nanotube membranes (CNM), an invention which is analogous to gold nanotube membranes but which has just recently begun attracting heavy interest. CNMs are prepared by template synthesis using nanoporous alumina templates which are commercially available and are grown in the lab as well. CNMs are an interesting and useful platform for the study of electroosmotic flow (EOF). In particular, the structural, physical, and chemical properties of nanotubes can be tailored using both the template method and electrochemical modification to exhibit nanofluidic control.

Template synthesis of CNMs entails chemical vapor deposition (CVD) of carbon into alumina membranes. The inherent flexibility of the method enables the CNM structural characteristics to be tailored to maximize permeability while maintaining good permselectivity. CNMs were prepared with pore diameters ranging from 10 to 200 nm and having either symmetric or asymmetric pore structures. Highly-ordered membranes

were prepared in which the nanotubes are near-perfect cylinders and extremely monodisperse in morphology.

EOF across template-prepared CNMs was used to modulate molecular transport. EOF in the direction of diffusion enhances transport across the membrane. However, EOF in the opposite direction diminishes, even eliminates, transport. In addition, the chemical and physicochemical properties of CNMs were tailored in order to control EOF by manipulating the experimental conditions. EOF was controlled and switched by adjustment of electrolyte concentration and pH as well as with the addition of small concentrations of surfactant.

The electrochemical capabilities of carbon nanotubes have also been used to tailor the properties of CNMs. Electromodified CNMs with a carboxylic functionality enhanced EOF while membranes with an amino functionality reversed it. Poly(phenylene oxide) nanotubes were grown inside carbon nanotubes by electropolymerization. EOF was passivated in these membranes even while diffusion and electrophoresis were still operative. A new approach for modulating EOF based on redox control of surface charge in poly(vinylferrocene) modified CNMs was demonstrated. The advantage of this method over other analogous electric-field methods is that it could be implemented with only a small battery for surface charge-control.

CHAPTER 1
INTRODUCTION – CARBON NANOTUBES TO NANOFLUIDICS

Carbon Nanotubes

Nanocarbons have been occasionally observed and studied for more than five decades.[1] In early years the nanocarbons observed were generally pyrolitic nanofibers or filaments and resulted from the decomposition of carbon-containing gases in the presence of catalytic metals.[2] However, in 1985, Smalley discovered a new class of highly-ordered molecular nanocarbons called buckminsterfullerenes in which sixty carbon atoms are arranged in a soccer ball-like structure.[3] The discovery of these new carbon molecules, nicknamed buckyballs, revolutionized how the world thought of carbon.

It was the study of buckyballs, using the arc-discharge process, that lead to the discovery by Iijima of carbon nanotubes (CNTs).[4] CNTs have been synthesized using a number of methods and in many different structural configurations. Generally speaking, most CNTs consist of graphene sheets rolled over into a cylinder and are capped with half buckyball-like structures at each end. The originally discovered fullerene CNTs (FCNTs) are classified as multi-walled nanotubes (MWNTs),[4] but later single-walled nanotubes (SWNTs) were observed as well.[5] As their name suggests, SWNTs consist of a single graphene cylinder with diameters as small as the theoretical limit of 4 Å[6] and as large as 3 nm or more.[7] SWNTs are very highly ordered and are often found to be structurally perfect. On the other hand, MWNTs contain many concentric cylinders with an interlayer spacing of 3.4 Å and have been prepared with outer-diameters ranging from ~1.4 nm to more than 100 nm. However, MWNTs are generally less well-ordered and

have been prepared with varying degrees of order or graphitization.[7]

In the 12+ years since their discovery, CNTs have become a major subject of attention in the research effort on nanoscale materials, and numerous outstanding reviews have been written on the subject.[7-18] It is a truism of nanoscience that as a material approaches molecular dimensions, its properties deviate from those of the bulk material. There may be no material for which this rule is truer than for carbon, as CNTs have been found to have many extraordinary properties.[19-23] For instance, FCNTs have been found to have either metallic or semiconducting properties depending on the direction that the graphene sheet is rolled.[19] In addition, FCNTs are capable of superconductivity with transition temperatures that increase with decreasing tube diameter.[20,21] Likewise, FCNTs are better conductors of heat than any other known material.[22] Finally, FCNTs possess exceptional mechanical properties as well; SWNTs are the strongest material by weight known and have been found to be more than 50 times as strong as steel wire.[23]

Because of the many novel properties of tubular carbon nanostructures, there are numerous potential applications using these materials. Some of these proposed uses include commercial composite materials,[8] nanoelectronics,[13,24-27] hydrogen storage,[28-30] electromechanical actuators,[31,32] Li-ion batteries,[33,34] chemical and bio-sensors,[35-37] AFM probes,[23,38] and field-emission devices.[39,40] Other novel applications will be the focus of the remaining chapters of this dissertation.

Synthesis of Carbon Nanotubes

Arc-discharge and laser ablation are two common methods of CNT synthesis. The arc-discharge and laser ablation processes use solid-state carbon precursors to provide carbon for nanotube growth. Both these methods can provide high-quality, even perfect nanotubes. However, combining the synthesis of high-quality CNTs with good

uniformity of size, quantity, and product purity has major limitations. Growth of large quantities tends to yield lower quality nanotubes in tangled masses randomly mixed with byproducts.[41] Various permutations of these methods have led to substantial progress, but SWNTs are produced only on a small scale and are quite expensive.[7] MWNTs are produced on a much larger scale but the product quality is a limitation for many applications as defect densities are quite high.[42]

Prior to the discovery of CNTs, nanocarbons were generally prepared using the chemical vapor deposition method (CVD).[2] Thus, it isn't surprising that CVD has become the third major method of CNT synthesis.[16,41] CVD allows growth-control opportunities that aren't available with arc-discharge or laser-ablation. The CVD method involves flowing hydrocarbon gas over a catalytic substrate at high temperatures (500 to 1000 °C). FCNTs are typically grown on catalytic transition-metal particles or "seeds" (most commonly iron, cobalt, or nickel). Carbon is partially soluble in these metals at high temperatures making them effective catalysts for CNT growth. The growth mechanism involves the dissociation of hydrocarbon molecules followed by the dissolution and saturation of carbon in the catalyst particle. Upon saturation, carbon atoms precipite from the catalyst solution. FCNTs are a lower energy form than other carbon allotropes, so carbon atoms precipitate into these tubular structures. MWNTs are easily formed using the catalytic-CVD method and have great potential for scaled-up production, as large-area, high-density arrays of tubes can be grown.[15] More challenging is the synthesis of defect-free SWNTs. This has been accomplished only recently and only in small scale.[43,44]

CVD offers several advantages over the more traditional arc-discharge and laser-

ablation CNT-growth technologies. First, nanotubes grow only on catalytic substrates; thus the location of CNT growth is controlled. Micro-patterning of catalyst substrate allows CNT growth in controlled locations and patterns.[41,45] Second, growing nanotubes are tethered to the catalyst material at one end, which allows implementation of directional, aligned growth-control strategies as well as direct electrical contact to the CNTs. These growth-control strategies include van der Waals interactions,[40] gas flow or "wind,"[46,47] and electric fields.[45,48] Third, the CVD rate is easily controlled and so works well with the general template synthesis method of growing nanostructures.[49-51]

The Martin laboratory, and others, have shown that carbon nanotubes can be grown by CVD of carbon along the pore walls of nanoporous templates.[33,52-57] This method results in free-standing, high density films or membranes of aligned nanotubes with monodisperse dimensions (Figure 1-1). The synthesis of these nanostructured materials and the template synthesis method in general are described in greater detail later in this chapter and in Chapter 2.

Carbon Membranes

Carbon has a long history of utility as membrane and filtration materials. Generally, these applications have used disordered, porous carbons such as activated carbon and pyrolytic carbon.[58] As a membrane material, carbon is of great interest due to its potentially high porosity and surface area, excellent thermal and chemical stability, low cost, and diverse array of available synthesis methods.[59]

Pyrolytic carbon membranes have been shown to be very effective for molecular sieving and selective surface flow separation schemes of gaseous mixtures.[59] The carbon membranes for gas separation are most commonly prepared by pyrolysis of various types of thermosetting polymer films.[60-63] The polymer is heated to high temperatures in a

reducing atmosphere where it breaks down into carbon and residual gases. The escape of these residual gases from the film results in a highly porous carbon membrane.

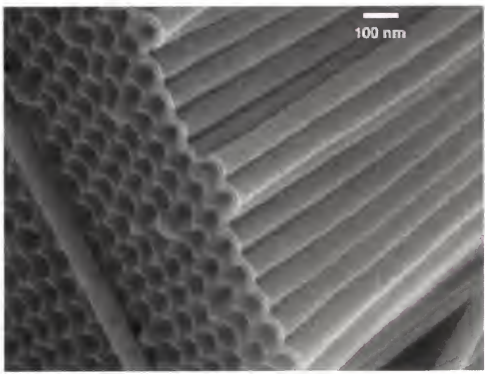

Figure1-1. Array of template-synthesized carbon nanotubes (scanning electron micrograph). The nanotubes were grown by CVD in a highly-ordered, lab-grown alumina template membrane.

Maximizing both the permselectivity and the permeability of a membrane, two parameters typically at odds with each other, is of primary importance in membrane design. Carbon molecular sieves (CMS), in which average pore sizes approach molecular dimensions are a good example of this.[59] High standards of pore-morphology control are needed to maximize transport-selectivity. In the case of CMS membranes, CVD of carbon has been used to narrow and homogenize pores to improve permselectivity.[64,65] However, Koros observed that with CMS separations of O_2/N_2, an increase in permselectivity of one order of magnitude corresponds to a decrease in permeability of six orders of magnitude.[66] In order to mitigate this permselectivity-permeability trade-

off, advanced membrane-design strategies must be employed to maximize pore density and minimize effective pore length and pore-size distribution. The most common design strategy to accomplish this is asymmetric membranes that have a very thin selective layer of fine pores on a large-pore support-membrane.[62,63,67] However, fabrication challenges make the preparation of defect-free films less than 100 nm in thickness very challenging.[66]

An interesting advantage of carbon as a membrane material is its electrical conductivity, which allows the membrane to also work as an electrode. Indeed, carbons in many forms have been used as electrode materials. For example, molecular-sieving, activated carbon electrodes have been used to study molecular sieving and surface adsorption by Soffer and co-workers in various media.[68-70] Of particular interest are results showing that carbon molecular sieves have proton-selective capabilities, which suggest that nanoporous carbons could be used as proton-selective membranes.[70] Other interesting potential uses for nanoporous membrane-electrodes demonstrated in noncarbon membranes include the electrochemical growth of composite membranes,[71,72] modification of pore chemistries,[71,73] and dynamic electrochemical control of transport phenomenon.[72-74]

At a recent workshop, it was suggested that carbon nanotubes might be used as chemically selective filters or membranes.[75] Indeed, a number of theoretical studies have been done investigating transport phenomenon within CNTs.[76-80] The carbon nanotube membrane (CNM) application[75] requires alignment of the open-ended tubes[40,81-83] into a defect-free, mechanically-strong membrane, where each tube spans the complete thickness of the membrane. There are numerous examples of aligned FCNT arrays,[16] but

none fulfill all of the above criteria.

Sun and Crooks recently developed an elegant procedure for preparing CNMs with a single MWNT.[84] However, template synthesis inherently provides nanotube-containing membranes of this type, with up to 10^{11} nanotubes per cm^2 of membrane surface area (Figure 1-1).[50] Having large numbers of nanotubes per cm^2 of membrane area is essential to maximizing permeability relative to permselectivity across the membrane, a critical issue in any membrane-separation processes.[66] Our lab, and others, showed that template-synthesized CNMs can be grown by CVD of carbon along the pore walls of nanoporous templates (Figure 1-2).[33,52,53,55,56] These CNMs are interesting electrode materials as well. To demonstrate their capabilities, we used the CNMs as Li^+ intercalation electrodes and as electrodes for electrocatalytic fuel-cell reactions.[32,33,85]

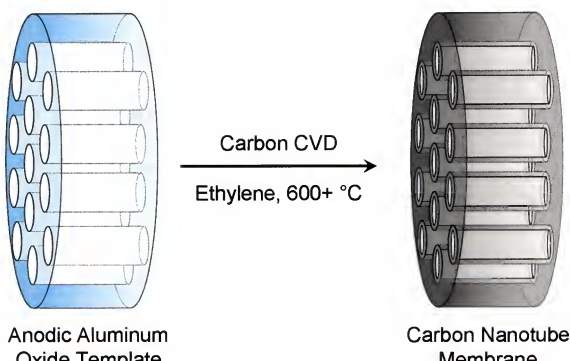

Figure1-2.Template synthesis of carbon nanotube membranes by CVD (schematic). A single carbon nanotube is conformally grown within each template pore.

The body of work reported in this dissertation is the first and, to date, the only demonstration and study of transport phenomenon in multi-tube CNMs. Additionally, using the membranes as electrodes we modified the pore chemistries of CNMs and grew composite-CNMs. In these composite-CNMs we demonstrated electrochemical dynamic control of transport phenomenon. These experiments constitute the first examples of their kind accomplished in CNMs, and each is discussed in detail in subsequent chapters.

Template Synthesis

Template synthesis, as a method for preparing 1-dimensional nanomaterials, was pioneered largely in the Martin laboratory in the late 1980s and early 1990s (Figure 1-2).[50,86,87] This method has its roots as far back as 1970, in work by Possin preparing metal nanowires.[88] The template method involves using the cylindrical nano- or micropores of membranes (Figure 1-3) as templates. Deposition of a material into the pores results in a parallel array of nanowires or nanotubes within the supporting template (Figure 1-2). Dissolving the template leaves a dense array of monodisperse nanostructures (Figure 1-1). The shape and outer diameter of the nanostructures are determined by the dimensions of the template pore itself. Control of deposition allows nanotubes to be grown with controlled wall-thicknesses.

The template synthesis method is very general;[49,50,89] it allows synthesis of nanostructures with diverse geometries composed of a great variety of materials.[49,50,89-93] The wide-ranging utility of template synthesis can be illustrated by contrasting superconducting SWNTs (with diameters of 4 Å, the finest CNT theoretically possible) grown in zeolite templates[21] with electrode-ensembles of vanadium pentoxide nanowires grown in polycarbonate track-etched membranes for high-rate, high-capacity batteries.[94]

Gold Nanotube Membranes

An interesting aspect of nanotubes prepared by the template-method is that the tubes can be left intact within the template resulting in a membrane in which each nanotube serves as a pore.[92] We call these template-prepared membranes "nanotube membranes" of which the first examples were gold nanotube membranes.[73,74,95] The gold nanotube-pores are prepared by electroless plating of gold onto polymeric track-etched membranes (Figure 1-3A).[96] Polymeric track-etched filtration membranes have proven to be very effective as templates over the years. Polycarbonate and polyester track-etched membranes are commercially available with a wide variety of pore diameters: from as small as 10 nm to greater than 1 μm. The pore densities are as great as 10^9 pores / cm^2 and the pore dimensions are very monodisperse. Interestingly, membranes with single pores have been prepared for investigation of transport and electrochemical phenomenon at the nanoscale.[97,98] In addition, track-etched membranes have been prepared in a number of materials other than polymers and with a similar range of pore densities.[99]

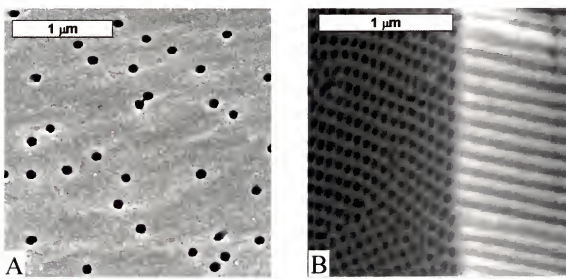

Figure1-3. Commonly used nanoporous template membranes (SEM micrographs). A) Polycarbonate track-etched membrane with 100-nm pores. B) Highly-ordered, home-grown anodic aluminum oxide membrane with 70-nm pores.

Gold nanotube membranes prepared in the polycarbonate track-etched membranes have proven accommodating to a number of novel applications in separations and as sensors.[100] For example, gold nanotubes have been grown with inner-diamters <1 nm.[95] Membranes of these nanotubes have been used as molecular sieves to separate molecules based on size. In other work, gold nanotube membranes have been set up as working electrodes and electrochemically charged in order to electromodulate transport.[74] In this configuration, each tube in the membrane approximates a narrow, charged capillary in which the diameter is smaller than the Debye length; hence, ions of like charge to the pore surface are electrostatically excluded from permeation through the membrane. Therefore, these membrane/electrodes allow selective transport of cations or anions purely as a function of electrode potential. In an extension of this experiment, surfactant counter-ions have been used to control the hydrophobic/hydrophilic nature of the pore, which allows electromodulated transport of neutral molecules based on hydrophobicity.[73] In addition, the chemical sensing abilities of gold nanotube membranes with pore diameters of 1-3 nm have been investigated.[101] Monitoring of either trans-membrane current or membrane potential has resulted in detection limits as low as 10^{-11} M.

Anodic Aluminum Oxide Template Membranes

Anodic aluminum oxide (AAO) nanoporous membranes (Figure 1-3B) are of particular interest to this dissertation as templates for carbon nanotube membranes (Figure 1-2).[53,54] AAO provides a great deal of design flexibility as templates; they are resistant to very high temperatures, mechanically rigid, and chemically stable in many media yet easily dissolved in solutions at high or low pHs. The flexibility of the template synthesis method with AAO templates has allowed synthesis of a number of interesting carbon devices, including Li^+ battery and electrocatalysis electrodes,[33,85] electrochemical

actuators,[32] nanoelectronic components,[57] and field emission devices.[102]

Commercially available Whatman Anodisc™ AAO filtration membranes have been used for a number of these applications.[32,33,53,54,85] These membranes are 60 μm thick, and contain a very high density ($1.2x10^9$ pores/cm^2) of generally cylindrical, parallel, and monodisperse pores.[103] Three types of Anodisc™ are available with "nominal" pore diameters of 20 nm, 100 nm, and 200 nm. However, these pore diameters are "nominal" as the pore diameters are actually 200-400 nm through ~99% of the membranes thickness. Near one face of the membrane, each of these long, large pores branch into many smaller pores of approximately the "nominal" diameter (Figure 1-4). Anodisc™ templates are very useful in that they are cheaply available in large quantities and are of consistent quality.

Figure 1-4. AAO membrane with asymmetric branched pores (illustration). Each pore branches into many smaller pores at one face of the membrane.

Since Anodisc™ templates are limited in available pore sizes and pore shapes, our lab and others commonly home-grow AAO templates as well (Figure 1-3B).[104-106] The AAO films are easily and inexpensively grown, with a wide variety of pore morphologies, either freestanding or supported on a substrate. For instance, straight-pore

templates with pore radii ranging from ~5 nm to ~200 nm, or asymmetric templates with large pores that branch into many much smaller pores at one face, can be prepared (Figure 1-4). In addition, AAO membranes can be grown as thin as 1 μm and/or with highly ordered, very monodisperse pores.

In the Martin lab, AAO membranes are grown by oxidation of high-purity aluminum metal using a two-electrode electrochemical setup (Figure 1-3B). The aluminum foil is used as the anode and is surrounded by a cylindrical stainless steel cathode. The electrolyte is a polyprotic acid, such as phosphoric or oxalic acid. Potentials ranging from 1 to 100 V are supplied by a variable power supply causing the formation an aluminum oxide film containing hexagonally packed pores. A nonporous layer of aluminum oxide, called the barrier layer, grows at the aluminum/AAO interface, separating the aluminum and porous alumina (Figure 1-5).

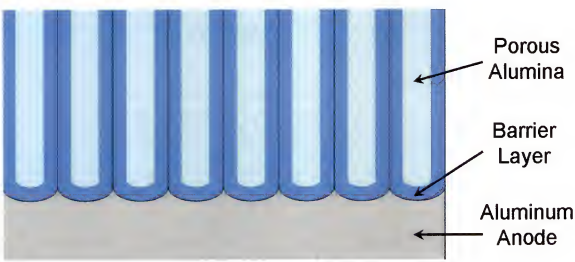

Figure 1-5. Porous anodic aluminum oxide film with barrier layer on aluminum anode (illustration). The electric field causes the aluminum to oxidize at the metal/oxide interface and enhances chemical dissolution at the base of the pores (i.e. at the barrier layer).

Pore growth is controlled as a function of the applied voltage: typically the pore size is ~1.4 times the voltage. However, to grow films with well-ordered, monodisperse

pores, the reaction must be kept slow (i.e., the current density should be constant and in the range of 1 to 6 mA cm^{-2}). To accomplish this, an appropriately conductive polyprotic acid is used as the electrolyte and the electrolyte solution is kept chilled to between 0 and 4 °C. Growth time is varied to control membrane thickness. While the tendency is for the alumina film to form a hexagonal array of uniformly shaped pores, the shape and location of the pore mouths is determined in large part by the topography of the aluminum surface. Naturally occurring pits and valleys on the aluminum surface serve as nucleation sites, and facilitate anodic pore growth.[107] As a result, the pores formed at the beginning of the growth process are somewhat randomly distributed with irregular shapes and sizes.

AAO membranes can be prepared with either straight-pore configurations or branched-pore configurations similar to the Anodisc™ membranes (Figure 1-4). For straight-pore alumina membranes, anodization is stopped when the porous alumina film reaches the desired thickness and the aluminum and barrier layers are chemically etched away. Alternatively, step-wise voltage reduction is used to form branched-pore membranes. As voltage is reduced, the growing pores will branch into many smaller pores with narrower alumina walls (Figure 1-4). Anodization will be stopped at a voltage at which the alumina walls are sufficiently narrow to quickly dissolve in an acid solution. The portion of the layer with the finest alumina walls will dissolve most quickly, leaving the remainder of the porous film intact and detached from the aluminum foil.

In a variation of the porous alumina growth method invented by Masuda, highly ordered "double-anodization" alumina membranes with very narrow pore size distribution have been grown.[106-109] These films have pores that are near-perfect

cylinders and are hexagonally packed (Figure 1-3B). Preparation of these membranes includes two anodization steps. The first step is a preliminary anodization in which the aluminum surface is anodized for several hours at the desired voltage. As the pores grow, they order themselves into the classical hexagonal packed array with a uniform size distribution. Cessation of the applied voltage stops pore growth. The alumina layer is dissolved in acid, leaving behind regularly dispersed, highly uniform indentations in the aluminum surface. Each indentation is a remnant of the aluminum/alumina interface at the bottom of a pore growth cell. Subsequently, in the second growth step under equivalent conditions, each indentation serves as a nucleation site for pore growth. Such double-anodization templates have highly ordered arrays of hexagonally-packed, discrete, parallel pores with very narrow size distributions.

Another method of producing "perfectly" ordered AAO has been developed by Masuda and coworkers.[110] In this method, a SiC stamp is fabricated by electron beam lithography with regularly-spaced, hexagonally-packed, convex bumps. By pressing the stamp into the aluminum metal, the aluminum prepatterned with ideally arranged nucleation sites for pore growth. The AAO films resulting from this method are amazingly well-ordered with nearly-perfect straight and monodisperse pores.

Electroosmotic Flow

Electroosmotic flow (EOF) is an interesting phenomenon of importance in many areas, particularly analytical chemistry and industrial separations. Analytical methods dependant on EOF include capillary electrophoretic methods, capillary electrochromatography, lab-on-a-chip electrophoresis analogs, and zeta potential surface analysis. Also, EOF is often used as a pumping mechanism for sample and reagent manipulation in lab-on-a-chip and other microfluidic devices. Electroosmosis is also

important in dewatering of soils and wastes, controlling leakage from waste sites, delivery of detoxifying agents, iontophoretic drug delivery, and industrial membrane separations such as desalination. EOF and other electrokinetic phenomenon are of particular interest to this dissertation as effective methods for modulating transport of solute molecules and ions across membranes.[53,74,111-114]

The Electric Double Layer

Most surfaces in water, including membranes, acquire surface charge due to mechanisms such as ionization, ion adsorption, and ion dissolution. The result of this charge is a surface potential that causes a shielding, ionic atmosphere to form in close proximity to the surface (Figure 1-6). Ions of opposite charge (counter-ions) are attracted to the surface while ions of like charge (co-ions) are repelled. Electroneutrality is violated in this ionic atmosphere, called the electric double layer, as it contains electrostatically-enhanced concentrations of counter-ions and diminished concentration of co-ions. The solution half of the electric double layer is composed of two layers of shielding counter-ions. Adjacent to the surface is the Stern layer – a single-ion-thick layer of immobile ions adsorbed to the charged surface. Outside the Stern layer is the diffuse layer – a thicker region containing mobile solvated ions. The interface between layers is the "plane of shear," where the mobile diffuse layer can flow past the Stern layer.

A major defining characteristic of the double layer is the zeta potential (ζ) which is defined as the potential at the plane of shear:

$$\zeta = 2kT/ze \sinh^{-1} (\sigma\kappa^{-1}ze/(2\varepsilon kT)) \qquad (1\text{–}1)$$

where k is the Boltzmann constant, T is temperature, z is the counter ion charge, e is the

elementary charge, ε is the permittivity of water, κ^{-1} is the Debye length or thickness of the double layer, and σ is the surface charge density at the plane of shear between the nanotube wall and the electrolyte. For relatively small zeta potentials that are relevant to this dissertation, Equation 1-1 simplifies to

$$\zeta = \sigma\kappa^{-1}/\varepsilon \qquad (1\text{-}2)$$

For a symmetrical electrolyte at 25 °C, κ^{-1} is related to the concentration of the electrolyte via

$$\kappa^{-1} = 9.61\text{x}10^{-9}(z^2c)^{-1/2} \qquad (1\text{-}3)$$

where c is concentration of electrolyte. It should be noted from Equation 1-3 that the double layer is thicker at lower electrolyte concentrations; ~1 nm for 0.1 M monovalent electrolyte and ~10 nm for 0.001 M. Bearing this in mind, the significance of Equation 1-2 is that in an aqueous environment, ζ increases with increasing surface charge and decreasing electrolyte concentration.

Electroosmotic Flow

Electroosmotic flow is the movement of liquid relative to a stationary surface by a tangentially applied electric field. The electric field applied along the charged surface causes the ions in the diffuse layer to migrate within the field. Because there is a larger concentration of counter-ions than co-ions in the diffuse layer there is a net migration of the counter-ions in one direction. In the case of the charged surface being a pore or capillary, water is drawn with the migrating counter-ions due to viscous drag. Mathematically, the Helmholtz-Smoluchowski equation describes the relationship between the velocity of electroosmotic flow (υ_{eo}, μm/s) and an electric field, E(x),

$$\upsilon_{eo} = -\varepsilon\zeta E(x) / \eta \qquad (1\text{-}4)$$

where η is the viscosity of the solution within the pore. It is implicit from Equation 1-2 and Equation 1-4 that a number of factors can be used to control EOF (principally surface charge, concentration and valency of electrolyte, and applied electric field strength).

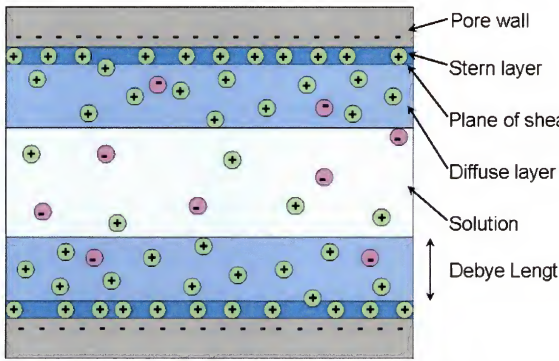

Figure 1-6. A negatively charged pore and the resulting electric double layer in electrolyte solution (illustration). The pore is viewed from the side.

It is an interesting exercise to contrast EOF with pressure-driven or hydraulic flow. One important characteristic of EOF is that the flow profile, across the cross-section of a pore, is flat or plug-like. This is because the force driving the flow occurs at the wall of the pore (i.e. the net migration of counter-ions in the diffuse layer). Therefore, the flowing diffuse layer "slips" by the pore wall at the plane of shear. In contrast, hydraulic flow is parabolic or laminar; since the driving-force, pressure, is spread across the entire pore cross-section, flow is stopped by friction at the pore walls, slowed near the pore walls, but relatively unhindered in the center of the pore.

This important difference also manifests itself in the relative efficiency of each

flow phenomenon as a function of pore radius. Electroosmotic flow rate is proportional to $\pi a^2 \upsilon_{eo}$ (where "a" is the pore radius) while hydraulic flow rate is proportional to $\pi a^4 \upsilon_{hy}$. This means that electroosmotic flow is relatively more effective in micro- and nano-scale pores while hydraulic flows are most effective at larger-scales (e.g. pipes). Another way to consider this reverse in efficiency is realizing that EOF is driven by forces at the water/wall interface, while hydraulic flow is slowed. Indeed, hydraulic flow is largely ineffective in many microfluidic applications at diameters below 10 μm.[115]

A limitation to the Helmholtz-Smoluchowski theory is that it assumes the solution in the pores approximates bulk solution; which isn't always true. For instance, as the capillary or average pore radius of a membrane approaches the dimensions of the electrical double layer (i.e. $\kappa^{-1} / a \approx 1$), electroneutrality is lost. In effect, the double layer completely fills the pore and the charged pore wall is never completely balanced by the counter-ions. In this case and in the case of particularly large zeta potentials, increased surface conductance and changes in permittivity or viscosity within the pores may cause deviations from the Helmoltz-Smoluchowski theory. Additionally, considering the case of $\kappa^{-1} / a \geq 1$, the electroosmotic driving-force is spread across the entire pore cross-section, and flow is slowed down by friction at the pore walls. Thus, in this instance, EOF is laminar instead of the plug-like flow it is most commonly associated with (i.e. the electroosmotic flow rate is proportional to $\pi a^4 \upsilon_{eo}$). The result is that EOF is less efficient and more difficult to control when $\kappa^{-1} / a \geq 1$.

Dynamic Electromodulation of Electroosmotic Flow

Dynamic electrochemical modulation of surface potential represents an interesting development and concept in separations research. Membrane-electrodes have been used

in a number of separations to modulate and control transport phenomenon.[72-74] In electrochemically-modulated liquid chromatography an electronically conductive stationary phase functions as the working electrode of an electrochemical cell.[116-119]. Charging the stationary phase allows manipulation of analyte retention. Stationary phase charging can be modified even during elution allowing quality-enhanced separations.

Electroosmotic flow has been modulated in capillaries and microfluidic chips by application of an external radial electric field across the capillary or micro channel wall.[115,120,121] In this work, the capillary was coated with an electrically conductive material and electrostatically charged as a working electrode. This external radial electric field has an additive effect on the native electric field originating from surface charge and allows positive, negative, or zero zeta potentials to be achieved through independent control of field strength. As zeta potential is directly related to electroosmotic flow velocity in a capillary by the Helmholtz-Smoluchowski equation (Equation 4), field-effect EOF modulation allows optimization of separations in capillaries and improved control of solutions on microfluidic chips.[115]

Control of EOF is very important in many separations techniques including capillary electrophoresis and electrochromatography, lab-on-a-chip electrophoresis, and a number of membrane-based methods. However, EOF control is of particular importance and is the method of choice for manipulating samples and reagents in the majority of microfluidic devices.[115,121] In addition, the interplay and control of EOF between nanoporous membranes and microchannels is of special interest in complex nano/microfluidic systems.[122,123]

Chapter Summaries

In Chapter 2 we demonstrate the key advantage to template synthesis: its inherent

flexibility in tailoring nanostructures with specific characteristics.[50] This method, as applied to synthesis of carbon nanotube membranes, entails growing carbon nanotubes by CVD of carbon into anodic aluminum oxide nanoporous membranes. The sizes and shapes of the nanotubes conform to those of their respective host pores.

Extensive control of carbon nanotube morphology and membrane characteristics has been exerted through careful selection of design parameters. CNM fabrication has been done with an eye towards maximizing both the throughput and the separation capabilities of the membrane. For instance, both symmetric and asymmetric CNMs have been prepared as a function of the type of template used and the CVD conditions. The asymmetric membranes have thin selective layers (<30 nm) which is important in maximizing permeability. Lab-grown AAO templates are particularly useful for fabricating CNMs with controlled nanotube dimensions. CNMs have been prepared with nanotube inside diameters as small as ~15 nm. Also, carbon nanotubes have been grown in highly ordered AAO that are near perfect cylinders and extremely monodisperse in morphology. Control of such highly-ordered, highly-uniform characteristics will be needed to fabricate good quality CNMs with very small inside diameters (<10 nm).

In Chapter 3 we describe the first example of electroosmotic flow in carbon nanotube array membranes.[53] EOF was driven across the CNMs by allowing the membrane to separate two electrolyte solutions and using an electrode in each solution to pass a constant ionic current through the nanotubes. EOF was investigated by measuring the flux of a probe molecule across the membrane. As-synthesized CNMs have anionic surface charge, and as a result, EOF was in the direction of cation migration across the membrane. EOF was used to modulate flux of the probe molecule. EOF in the direction

of the diffusing probe molecule enhanced flux across the membrane. Reversing EOF (i.e. in the opposite direction of diffusion) diminished flux, even turning transport off at high EOF velocities.

The EOF characteristics of the CNM were modified by changing the pH of the electrolyte. The point of zero charge, pzc, was determined to be pH 3.5. EOF at pH < 3.5 was reversed respective to EOF at pH >3.5. EOF was controlled dynamically in CNMs with the addition of cationic surfactant to the permeation cell solutions. Due to the anionic surface charge on the nanotube wall, the surfactant self-assembled into a cationic bilayer giving the membrane a net cationic surface charge. As a result, once the surfactant-bilayer formed, EOF in the CNM reversed directions.

In the work reported in Chapter 4, we take advantage of the electronic conductivity of carbon nanotubes to modify the inner walls of the tubes. Our goal for modifying CNMs was to alter and control the EOF properties of the membranes. For instance, we used an electrochemical derivatization method to attach carboxylate groups to the nanotube walls; this enhances the native anionic surface charge, resulting in a corresponding increase in the zeta potential and EOF rate. Electrochemical derivatization was also used to attach cationic ammonium sites to the nanotube walls to yield CNMs that show EOF in the opposite direction of the as-synthesized and carboxylated membranes.

We have also used electrochemical polymerization methods to prepare carbon nanotube-polymer composite membranes.[124,125] In membranes modified with polyphenylene oxide (PPO), EOF was passivated. However, the nanotubes remained open allowing diffusion and electrophoretic migration through the membrane. In other

CNMs, modified with the redox-active polymer poly(vinyl ferrocene) (PVFc), we demonstrated a new system of dynamic EOF control. We reasoned that surface charge of a nanotube modified with a redox-active species, such as ferrocene, could be controlled based on redox state. Thus, EOF could be electrochemically redox-modulated in such a membrane (Figure 4-1). This is a new method of dynamic EOF control that has not been previously demonstrated.

CHAPTER 2
SYNTHESIS AND TAILORING CARBON NANOTUBE MEMBRANES BY THE TEMPLATE METHOD

Introduction

Carbons have a long history of utility as membrane and filtration materials. Generally, these applications have used disordered, porous carbons such as activated carbon and pyrolytic carbon.[58] As a membrane material, carbon is of great interest due to its potentially high porosity and surface area, excellent thermal and chemical stability, low cost, and diverse array of available synthesis methods.[59,66] Another interesting but under-utilized advantage of carbon as a membrane material is its electrical conductivity.[68-70]

Maximizing the permselectivity and the permeability of a membrane, two parameters typically at odds with each other, is of primary importance in membrane design.[66] Carbon molecular sieves in which average pore sizes approach molecular dimensions are a good example this.[59,66] Koros observed that with carbon molecular-sieving separations of O_2/N_2, an increase in permselectivity of one order of magnitude tends to correspond with a decrease in permeability of six orders of magnitude.[66] In order to mitigate this permselectivity-permeability trade-off, advanced membrane design strategies have been employed to maximize pore densities, minimize effective pore lengths, and narrow pore-size distributions. For instance, chemical vapor deposition (CVD) of carbon has been used to narrow and homogenize pores to improve permselectivity.[64,65] Another more common strategy is to design asymmetric

membranes that have very thin selective layers of fine pores on a large-pore support-membrane.[62,63,67] Historically though, fabrication of defect-free films less than 100 nm in thickness is very challenging.[66]

At a recent workshop it was suggested that aligned arrays of carbon nanotubes might be used as membranes in which the nanotubes serve as pores.[75] Indeed, a number of theoretical studies have been done investigating transport phenomenon within carbon nanotubes.[76-80] The carbon nanotube membrane (CNM) application[75] requires alignment of the open-ended tubes into a defect-free, mechanically-strong membrane, where each tube spans the complete thickness of the membrane. Sun and Crooks have recently developed an elegant procedure for preparing CNMs but only with a single multi-walled nanotube.[84] However, template synthesis inherently provides nanotube-containing membranes of this type, with up to 10^{11} nanotubes per cm^2 of membrane surface area.[49,50] The Martin laboratory, and others, have grown CNMs by CVD of carbon along the pore walls of nanoporous templates (Figures 1-1 and 1-2).[33,52,53,55,56]

The first example of nanotube membranes were template-prepared gold nanotube membranes,[73,74,95] an interesting analog to CNMs. Gold nanotube membranes are prepared by electroless plating of gold into the pores of polymeric track-etched template membranes.[96] The key feature which makes gold nanotube membranes so interesting is that the gold nanotube inner-diameters are "tunable" (i.e. pore-size can be controlled). Membranes have been prepared with nanotube i.d.s ranging from >100 nm to <1 nm, the smallest of which act as molecular sieves.[95] Small molecules in solution permeate through the membrane while larger molecules are not transported at detectable levels. Control of nanotube dimensions is of utmost importance in such size-based separations;

but it has also proven to be equally important in chemical-selective[73,126] and ion-selective[74,127] methods of separation as well.

In this chapter we demonstrate the key advantage to template synthesis: its inherent flexibility in tailoring nanostructures with specific characteristics.[50] This method, as applied to synthesis of carbon nanotube membranes, entails growing carbon nanotubes by CVD of carbon into anodic aluminum oxide nanoporous membranes (Figures 1-1 and 1-2). The sizes and shapes of the nanotubes conform to those of their respective host pores.

Extensive control of carbon nanotube morphology and membrane characteristics has been exerted through careful selection of design parameters. CNM fabrication has been done with an eye towards maximizing both the throughput and the separation capabilities of the membrane. For example, both symmetrical, straight-pore CNMs and asymmetrical, branched-pore CNMs have been prepared as a function of the type of template used. In addition, carbon layer growth has been controlled as a function of the CVD rate and duration. At low CVD rates, carbon deposition is uniform and nanotube wall thickness is easily controlled as a function of CVD duration. However, at high CVD rates, carbon deposition is diffusion-limited and occurs preferentially at the mouths of the pores. This results in bottlenecking at the nanotube ends, giving the membrane an ultra-thin selective layer of less than 30 nm. Lab-grown AAO is particularly useful for fabricating CNMs with controlled nanotube dimensions. CNMs have been prepared with nanotube inside diamteters as small as ~15 nm. Also, highly-ordered AAO membranes were grown with very uniform pores. Carbon nanotubes grown in these template are near perfect cylinders with ~50 nm inside diameters and are extremely monodisperse in

morphology. The ability to grow such highly-ordered, highly-uniform pores will be needed to fabricate good quality CNMs with very small nanotubes (<10 nm).

Expermimental

Materials

Ethylene (30% in helium) and argon were used as received. Two types of Whatman Anodisc™ Filter Membranes, designated as having either 20 nm or 200 nm diameter pores, were used as templates (Chapter 1). The carbon nanotubes discussed in this chapter were prepared in the 200-nm templates unless otherwise stated. Lab-grown anodic aluminum oxide (AAO) template membranes with pore diameters of 30 nm and 70 nm were used as well (Chapter 1).

Preparation of Carbon Nanotube Membranes

The preparation of the carbon nanotube membranes has been described previously.[33,53,55] Prior to CVD synthesis, the AAO membranes were sandwiched between two quartz plates, and heated to a temperature slightly higher than the CVD temperature for 30 min in air. If this heat pretreatment is not done, the alumina membranes curl into a tight cylinder during the CVD synthesis of the carbon membrane. Heat pretreatment between quartz plates prevents this unwanted curling, and allows synthesis of planar carbon-containing membranes.

A 3.5 x 1.5 cm piece of the alumina template membrane was placed in the CVD reactor and the reactor temperature was increased to the CVD temperature, 650 – 870 °C, under argon flow. The CVD temperature was varied from membrane to membrane as needed to control CVD kinetics. When the temperature stabilized, the Ar flow was terminated, and simultaneously a 20-sccm flow of ethylene was initiated. Ethylene decomposes within the pores of the template membrane to yield the desired carbon

nanotube membrane (Figure 1-2). The amount of carbon deposited (i.e., the thickness of the walls of the carbon nanotubes and the surface layers) is controlled by the deposition time and temperature. After deposition, the Ar flow was resumed, the ethylene flow was terminated, and the furnace was turned off and allowed to cool to room temperature.

Electron Microscopy

Scanning electron microscopy (SEM) and transmission electron microscopy (TEM) were used to image the carbon nanotubes prepared within the pores of the alumina template membrane. This was accomplished by first dissolving away the alumina by immersion in concentrated HF for 12 hours. The HF was removed by pipette leaving the liberated nanotubes (connected together by the carbon surface films), which were rinsed and then suspended in methanol. This suspension was then ultrasonicated for 20 min.

For the preparation of SEM samples a drop of the ultrasonicated membrane suspension was applied to a copper foil adhered to a SEM stub and the solvent was allowed to evaporate. Gold was sputtered onto the sample in order to improve electrical conductivity. Images were obtained using a JEOL 6335F field emission gun microscope. For TEM imaging a drop of the suspension was applied to a Carbon Type A TEM grid. The carbon nanotubes adhered well to the grid and were easily imaged using a JEOL 2000 microscope.

Results and Discussion

Template Synthesis of Carbon Nanotube Membranes

Figure 2-1 shows SEM images of each face of a 200-nm Anodisc™ template. At the unbranched face of the membrane the pore mouths are circular and ~300 nm in diameter on average (Figure 2-1A). At the branched face of the membrane the pore mouths are irregularly shaped with diameters ranging from 100 – 200 nm (Figure 2-1B).

Each of these pores serve as a template in which a carbon nanotube is grown (Figure 1-1). Thin films of carbon are deposited by CVD on the pore walls forming nanotubes. The shape and dimension of each nanotube is determined by the morphology of the pore it is grown in.

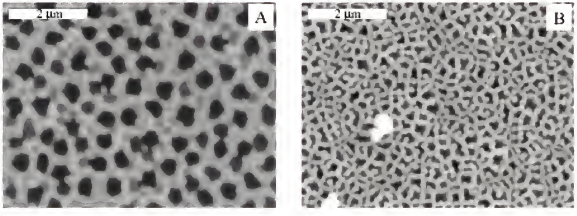

Figure 2-1.200-nm Anodisc™ template membrane (SEM micrograph). (A) Unbranched face with ~300 nm pores. (b) Branched face with 100-200 nm pores.

Figure 2-2A shows a cross-sectional image of the CVD carbon nanotubes after dissolution of the alumina template. A parallel array of nanotubes is obtained because the tubes are connected together by the carbon surface film that can be seen at the top of the image. However, these surface films have the same thickness of the carbon nanotube wall and are rather delicate. For this reason the template is left in place to support the membrane structure for most applications.[32,53] While it is not evident from this image, the carbon surface film does not block the mouths of the nanotubes.

Figure 2-2B shows a TEM montage image of individual carbon nanotubes that had become separated from the carbon surface films during ultrasonication of the nanotube suspension. This image also shows that the tubes have a consistent wall thickness down their entire length; a wall thickness value of ~40 nm was obtained from such images. Clearly, the outside diameter of the nanotubes (~300 nm) is larger than the nominal 200

nm pore diameter of the template. Our SEM and TEM images indicate that this is because the pores are, in fact, larger than the nominal diameter for most of the thickness of the membrane but branch at one face of the membrane into smaller (diameter ~100-200 nm) pores (Figure 1-4). This branching can also be seen in the TEM image shown in Figure 2-2B. Branching undoubtedly results from the voltage reduction technique used during the final voltage reduction step of the electrochemical process used to prepare these alumina membranes (Chapter 1).[128] Permeation experiments, described in Chapters 3 and 4, have repeatedly and reproducibly shown that these CNMs have porosities of 18-22%.

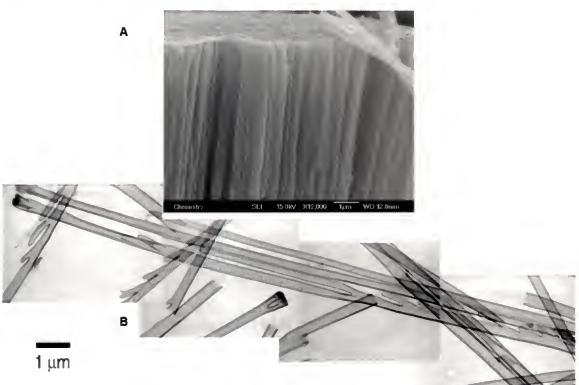

Figure 2-2. Carbon nanotubes grown by CVD in 200-nm Anodisc™ template membrane (electron micrographs). (A) SEM image of a CNM cross-section after removal of the alumina template. (B) TEM image montage of individual carbon nanotubes removed from a CNM.

While nanotubes prepared in the 200-nm Anodisc™ template are less than perfect cylinders, these membranes are commercially available with consistently uniform characteristics. More importantly, the nominal 120 nm diameter of these carbon nanotubes is ideal for electroosmotic flow. The EOF control experiments reported in Chapters 3 and 4 are all carried out using carbon nanotube membranes prepared in these templates.[53]

Effect of High CVD Rate on Carbon Nanotube Growth

It is well known that CVD reactions are more rapid at higher temperatures.[129] Figure 2-3 shows TEM images taken at the end and the middle of a single nanotube that was grown in a 200-nm Anodisc™ template (Figure 2-1) at a high CVD temperature (870 °C). At the end of the nanotube, the carbon walls become thicker and form a bottleneck-like structure (Figure 2-3A). The bottleneck of the nanotube is very short, <30 nm, and is more than 10x narrower than the majority of the tube. Bottleneck pore structures such as these are of interest for designing membranes which maximize both permeability and permselectivity.[66]

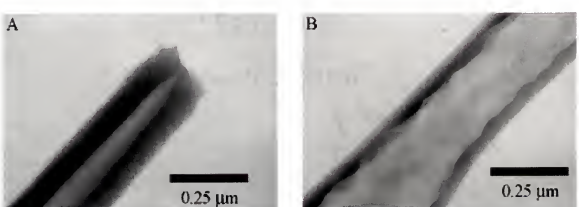

Figure 2-3. Carbon nanotube grown at a high CVD rate in 200-nm Anodisc™ template (TEM micrographs). (A) Image of nanotube end. (B) Image of approximate midpoint of nanotube.

From Figure 2-3B it is clear that the nanotube walls towards the midpoint of the tube are much thinner and less uniform than at the end of the nanotube (Figure 2-3B). This non-uniform carbon-wall thickness observed along the length of the nanotube is in stark contrast to what was observed for nanotubes grown at 670 °C (Figure 2-2B). The nanotube walls grown at the lower temperatures, thus lower deposition rates, are highly uniform along the length of the tubes as well as from tube to tube. Undoubtedly, this disparity is due in large part to the preferential deposition of carbon at the template pore openings because of mass-transfer limitations.[65] At the higher CVD temperature, the vapor deposition reaction occurs too rapidly for diffusion to maintain equilibrium and a concentration gradient develops along the length of the template pore. It should be noted that the diffusion-limited CVD phenomenon is exacerbated as the carbon nanotube pores become narrower.

Characterization of the CVD Template Method

Certainly, control of carbon deposition is important in preparing CNMs with tailored properties. In order to gain a quantitative understanding of the growth process, membranes were weighed before and after deposition of carbon. We define the ratio of the mass of carbon to the mass of AAO as %Carbon:

$$\%\text{Carbon} = (m_{fin} - m_{init}) / m_{init} \cdot 100\% \qquad (2\text{-}1)$$

where m_{init} is the mass of the template and m_{fin} is the mass of the membrane after nanotube growth.

Figure 2-4 shows a plot of %Carbon (Equation 2-1) vs. t_{CVD} (where t_{CVD} is the duration of CVD in minutes) for CNMs grown at 730 °C (a temperature where deposition is largely uniform). At relatively short deposition times (up to ~6 hours), there is an

approximately linear relationship. This is not surprising as the mass of carbon deposited should be closely related to surface area of the substrate.[129] Interestingly, at longer deposition times, %Carbon abrubtly stops increasing. This would seem to indicate that carbon deposition has likewise stopped. However, another possibility is that this is due to a large drop in surface area as the nanotubes are near-simultaneously closed by carbon growth. This is quite plausible, as calculation and experiment have shown that the pore walls comprise at least 99.5% of the total surface area of 200-nm Anodisc™ membranes.[103] The %Carbon maximum is approximately the same for all "low-temperature"depositions indicating that the second scenario is even more likely.

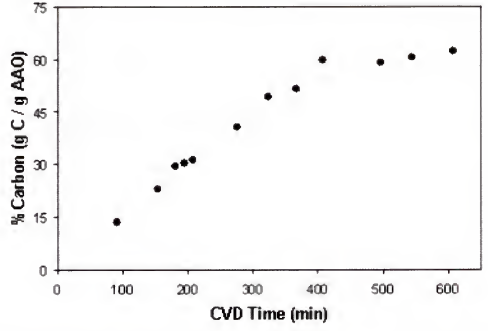

Figure 2-4. %Carbon vs. CVD time for carbon nanotube membranes synthesized at 730 °C.

In principle, the slope of the %Carbon – t_{CVD} relationship (Figure 2-4) at any time is the rate of carbon deposition. While the actual rate of carbon deposition is not linear over all times (Figure 2-4) the approximation can be made that the CVD rate is constant at short times. This allows average CVD rate, R_{CVD}, to be calculated from %Carbon

$$R_{CVD} = (m_{fin} - m_{init}) / (m_{init} \cdot t_{CVD}) \qquad (2\text{-}2)$$

with R_{CVD} having the units g C / (g AAO · min). Figure 2-5 shows a plot of R_{CVD} vs. CVD Temperature. These data points are all from CNMs with %Carbon less than 40. Clearly CVD temperature is an integral parameter for controlled growth of CNMs as R_{CVD} increases rapidly with temperature. It should be remembered that at higher temperatures deposition approaches the diffusion-limited regime and is not completely uniform (Figure 2-3). However, TEM analysis showed that this effect is not very pronounced even at 770 °C.

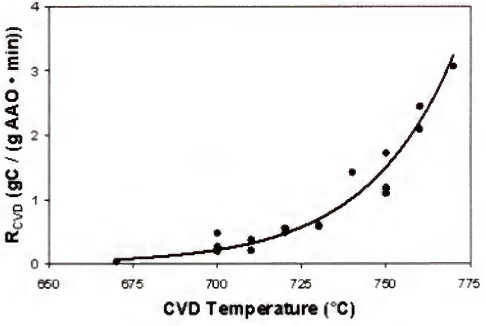

Figure 2-5. Average rate of carbon deposition vs. CVD temperature for carbon nanotube membranes. All CNMs were less than 40 %Carbon.

Branched Carbon Nanotubes

Figure 2-6 shows images of a CNM synthesized within a highly asymmetric Anodisc™ 20-nm filtration membrane. Like the 200-nm template, this template has large pores (diameters of ~300 nm) along ~99% of their length but branch into many much smaller pores (diameter ~20 nm) at the branched face of the membrane (Figure 1-4).

CVD was done at 900 °C for 0.5 hours, which resulted in a much more rapid rate of carbon deposition.

At this high temperature, deposition was very much into the diffusion-limited CVD regime. Therefore, deposition was much more rapid at the face of the template as opposed to within the small pores. This can be seen by contrasting the substantial surface film seen at the branched-face in Figure 2-6A with the thin nanotube walls seen in Figure 2-6B. Surely the nanotubes are closed over by the surface layer in this membrane as a result. Interestingly, such CNMs act as electrochemical actuators. The membranes bend back and forth when Li^+ is intercalated into and deintercalated out of the carbon nanostructures.[32] Grown at lower temperatures, such highly-branched carbon nanotube membranes have very narrow pores of minimal length. These types of branched-CNM are capable of much higher fluxes than membranes with straight pores of similar size.

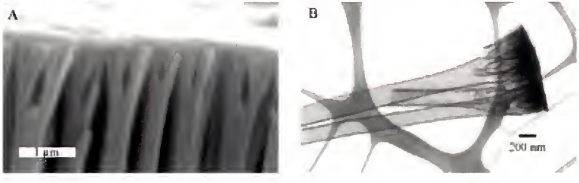

Figure 2-6. Carbon nanotubes grown at a high CVD rate in 20-nm Anodisc™ membrane (electron micrographs). (A) SEM image of the branched side of a CNM cross-section after removal of the alumina template. (B) TEM image of branched-ends of several nanotubes.

Carbon Nanotube Membranes Prepared in Lab-Grown Alumina

While convenient to use and having many useful characteristics, Anodiscs™ are limited in the number of pore-sizes and pore-shapes available. For that reason, lab-grown AAO templates have been prepared in the Martin laboratory with a wide variety of pore

morphologies for a number of different applications (Chapter 1).[105,108] Figure 2-7 shows a TEM micrograph of very narrow carbon nanotubes (i.d. ~15 nm) that were grown in an AAO template with straight ~25 nm pores. CVD was done at 700 °C and as expected the nanotube walls are very uniform in thickness despite aspect ratios of the template-pores being >1000. Such controlled CVD in lab-grown AAO allows CNMs to be prepared with a wide range of inner and outer nanotube diameters.

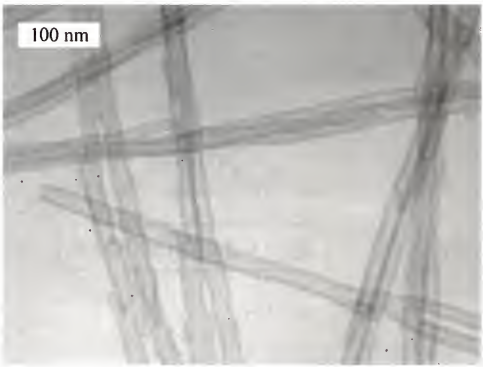

Figure 2-7. Carbon nanotubes grown at 700 °C in a lab-grown AAO template (TEM micrographs).

A limiting factor, with both types of AAO template discussed so far, is that the pores are not truly monodisperse (i.e. not completely uniform in dimensions). While this is generally not a problem in areas of study requiring large pores (e.g. electroosmotic flow[53] or energy storage/production electrodes[33,85]), it becomes more of a concern in experimental investigations of modeled transport systems[76,77,79,80] and membranes where pore-requirements approach molecular dimensions (i.e. <10 nm).[73,74,95] A new double-

anodization method was recently been developed for growing very highly ordered AAO templates (Chapter 1).[106,108] Figures 2-8A and B show SEM images of one such double-anodization membrane. Clearly the template pores are very straight and cylindrical through the thickness of the membrane, as well as, highly uniform in size and shape.

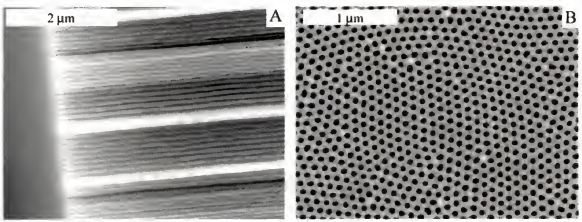

Figure 2-8. Lab-grown double-anodization AAO membrane (SEM micrographs). (A) Cross-section with pores running from left to right. (B) Solution face of the membrane.

Double anodization templates allow synthesis of highly-ordered carbon nanotube membranes with very monodisperse nanotubes as shown in Figure 1-1. Figure 2-9A shows a SEM image of the face of the same highly-ordered CNM. The carbon nanotubes are open-ended with highly monodisperse inside-diameters. Figure 2-9B shows a TEM image of a carbon nanotube removed from the membrane. The CVD temperature was low (670 °C) for this CNM, so as expected, the nanotube walls are very uniform in thickness. Varying the duration of the CVD step results in thicker or thinner nanotube walls and, therefore, CNMs can be tailored with narrower or wider pore sizes.

Conclusions

Anodic aluminum oxide template membranes can be purchased or lab-grown with a wide variety of pore morphologies. Highly-porous, template-prepared carbon nanotube

membranes have been synthesized by CVD of thin carbon films into AAO templates. Using this method, carbon nanotubes are grown in each template pore and likewise conform to the shape and dimensions of the host pore. Each nanotube has an inner diameter defined by the thickness of the tube-wall and diameter of the template pore. The CNMs contain very dense parallel arrays of monodisperse carbon nanotubes.

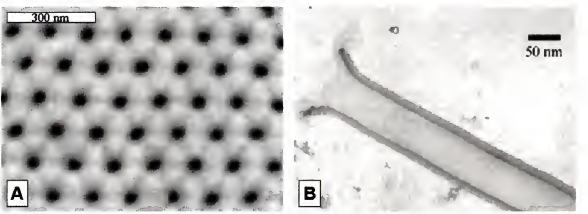

Figure 2-9. Carbon nanotubes grown in a home-grown double-anodization AAO membrane (electron micrographs). (A) SEM image the CNM face. (B) TEM image of a single nanotube isolated from the CNM.

Synthesis of high-throughput, high-selectivity membranes requires very fine control of pore morphology. A number of synthesis strategies have been used to prepare carbon nanotube membranes containing nanotubes with a variety of shapes and sizes. CNMs with pore diameters >100 nm and ~20% porosities have been reproducibly grown for EOF studies.[53] CVD at high temperatures results nanotubes with bottlenecks at their ends. Bottlenecked-CNMs are asymmetric with very thin selective layers of <30 nm. Another strategy used for preparing asymmetric CNMs was to grow nanotubes in a template with highly branched pores. The ability to grow such highly porous membranes with asymmetric pore structures is very important in maximizing permeability while maintaining good selectivity.[66] However, above all, preparation of a high-performance membrane requires very small and very uniform pores. Nanotubes have been prepared in

lab-grown AAO with inner diameters as small as ~15 nm. CNMs grown in double-anodized AAO contain extremely monodisperse nanotubes. Undoubtedly, the combination of such high quality AAO templates with controlled CVD will enable the tailored-growth of CNMs with a wide variety of properties and capabilities.

CHAPTER 3
ELECTROOSMOTIC FLOW IN TEMPLATE-PREPARED CARBON NANOTUBE MEMBRANES

Introduction

Carbon nanotubes are of great current interest in both fundamental and applied science.[24-27,29,30,33,40,130,131] Potential applications for these tubular nanostructures include use in nanoelectronics,[24-27] hydrogen storage,[29,30] and battery[33,130] and field-emitting-display[40,131] technologies. We, and others, have shown that carbon nanotubes can be prepared via the template method [49-51] by doing chemical vapor deposition of carbon along the pore walls of microporous alumina membranes (Figure 1-2).[32,33,56,85] These membranes have cylindrical pores with monodisperse diameters, and a corresponding cylindrical nanotube is deposited within each pore. Carbon nanotubes with outside diameters as small as 20 nm have been prepared via this method.[56] Using an alternative template material and method, Joo et al have prepared carbon nanotubes with outside diameters of 9 nm.[130]

At a recent workshop it was suggested that carbon nanotubes might be used as chemically selective filters.[75] This membrane-separations application will require alignment of the tubes[40,81-83] into a defect-free, mechanically-strong membrane, where each tube spans the complete thickness of the membrane and the tube mouths are open at the membrane faces. While Sun and Crooks have recently developed an elegant procedure for doing this with a single carbon nanotube,[84] template synthesis inherently provides nanotube-containing membranes of this type, with up to 10^{11} nanotubes per cm^2

of membrane surface area.[50] Having large numbers of nanotubes per cm^2 of membrane area is essential to enhancing flux across the membrane, a critical issue in any membrane-separation processes.

Flux can also be enhanced by augmenting diffusive transport across the membrane with electrophoresis or with pressure-driven or electroosmotic flow. Sun and Crooks demonstrated diffusive, pressure driven and electrophoretic transport of colloidal particles across their single carbon-nanotube membranes.[84] We describe here the first example of electroosmotic flow (EOF) in carbon nanotube array membranes.[53] EOF can be driven across the carbon nanotube membranes (CNMs) by allowing the membrane to separate two electrolyte solutions and using an electrode in each solution to pass a constant ionic current through the nanotubes. As per White et al., EOF was investigated by measuring the flux of a probe molecule across the membrane.[112,113] The as-synthesized CNMs have anionic surface charge, and as a result, EOF is in the direction of cation migration across the membrane. EOF was reversed dynamically in CNMs with the addition of cationic surfactant to the permeation cell solutions. Due to the anionic surface charge on the nanotube wall, the surfactant self-assembles into a cationic bilayer giving the membrane a net cationic surface charge.[132]

Experimental

Materials

Whatman Anodisc microporous alumina filters were used as the template membranes. Argon, nitrogen, phenol, hexadecyltrimethylammonium chloride (HTAC), and sodium chloride were used as received. A 30:70 (v/v) mixture of ethylene and He was used for CVD of the carbon nanotubes. Purified water was prepared by passing house-distilled water through a Millipore Milli Q water purification system. Buffer

solutions were prepared from monobasic sodium phosphate and adjusted to pH 7.2 with 1 M NaOH.

Preparation of the Carbon Nanotube Membranes

The CVD method used has been described in general previously in Chapter 2 and elsewhere.[33,53,55] The specific procedure for the membranes studied in this chapter is briefly described here. Prior to CVD synthesis, the alumina template membranes were pre-treated at 740 °C for one hour. This was done to prevent unwanted curling, and allowed synthesis of planar CNMs. The template membrane was placed vertically in the reactor and CVD of carbon was done at 670 °C for 5.5 hours. After CVD, the Ar flow was resumed, the ethylene flow was terminated, and the CNM was allowed to cool to room temperature.

After synthesis the membranes were stored in air for at least 24 hours prior to use. This results in oxidation of the carbon surfaces to yield acidic surface sites on the nanotube walls.[133-135] CNMs treated in this way are referred to as "as-synthesized" membranes. Four different membranes were used for the studies reported here. However; many more were characterized and the success rate for preparing these membranes approached 100%.

X-Ray Photoelectron Spectroscopy (XPS)

XPS studies of the samples were performed on a Kratos XSAM 800 spectrometer using Mg K_α excitation (200 W). The samples were mounted onto a stainless steel sample stub by means of a 7 mm diameter carbon sheet disk (SPI Supplies), so as to completely cover both the carbon disk and the sample stub. The samples were inserted into the sample analyzer chamber by means of a quick insertion probe, and spectral acquisition using the fixed analyzer transmission mode commenced after the pressure

decreased to $5x10^{-9}$ torr. Survey scans, high-resolution C 1s spectra and high resolution O 1s spectra were recorded at a take-off angle of 20° relative to the sample surface. The information depth (99% criterion, calculated as 3D, where D is the mean escape depth)[136] is estimated as 2.5 nm for C 1s. Data analysis was done using the DS 800 software package. Peak positions were all referenced to 285.0 eV for the main carbon peak.

Permeation Measurements

The CNM was mounted in the supporting assembly shown in Figure 3-1A. After assembling the various components, the assembly was heated for three minutes at 150 °C in an oven to melt the Parafilm, which acted as a glue to hold the various pieces together. This assembly exposes a 0.713-cm^2 portion of the CNM to the electrolyte solution. Electroosmotic flow (EOF) measurements were made in a U-tube permeation cell shown in Figure 3-1B. The membrane assembly was clamped between the two halves of the U–tube cell and both half-cells were filled with 25 mL of pH = 7.2 phosphate buffer. Unless otherwise stated, the ionic strength of the buffer solutions was 0.01 M. The resistivities of the electrolyte solutions used were determined using an Accumet AR-50 conductivity meter.

An EG&G 173 galvanostat was used to pass a constant ionic current through the CNM. This current was responsible for EOF in the membrane. The rate and direction of EOF was varied by varying the magnitude and sign of the applied current. The faradaic reactions occurring at the Pt electrodes (which support the ionic current in the nanotubes) were simply the reduction and oxidation of water. The alternative to this constant current approach would be to apply a constant transmembrane potential. However, in this case, the voltage drop across the membrane would have to be independently determined.

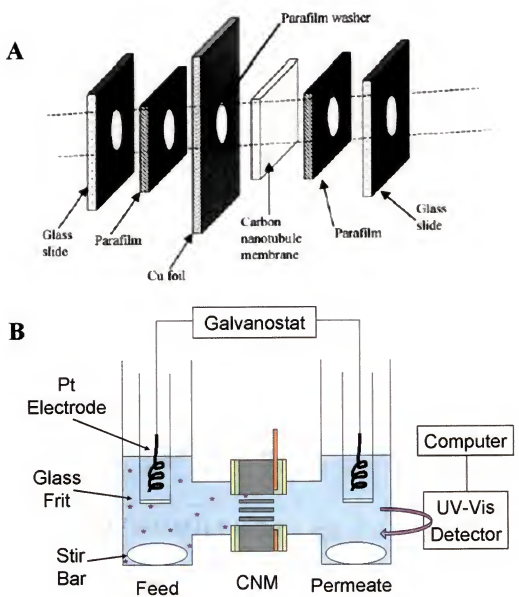

Figure 3-1. CNM permeation cell setup schematics (illustrations). (A) Exploded view of the nanotube membrane assemply. The holes in glass slides and Parafilm are 0.95 cm across. The hole in the Cu foil is 1.27 cm across. (B) Schematic of permeation cell used for EOF experiments.

The following sign convention was employed: For a positive applied current, the anode was in the feed half-cell and the cathode was in the permeate half-cell. In this case, cations migrated from feed to permeate and anions from permeate to feed. A negative applied current had the opposite configuration; i.e., cathode in the feed half-cell

and anode in the permeate half-cell. The current values are reported here as the current density, defined as the applied current divided by the total pore area of the membrane.

The feed half-cell was 4.82 mM in the small, electrically neutral, chromophoric probe phenol. As per Bath et al.,[112,113] the rate of EOF was determined by monitoring the transport of the probe molecule across the membrane and into the permeate half-cell. This was accomplished by continuously pumping the permeate solution through a Waters 486 HPLC UV/visible detector set at 270 nm (an absorbance maxima for phenol). An Eldex Laboratories AA-100-S piston pump was used to circulate permeate solution through the detector. Absorbance data were obtained at a rate of 20 points per minute. These data were logged on a PC interfaced to the absorbance detector. The absorbance data were converted to moles of phenol transported with the aid of a calibration curve. These data were processed as plots of micromoles phenol transported vs. time. The plots appear as uninterrupted lines because of the large quantity of data obtained. The total pore area was determined from the known diffusion coefficient for phenol in water at 298 K (9.68×10^{-6} cm^2 s^{-1}),[137] the known concentration gradient of phenol across the membrane, and the measured diffusive flux (no applied current) of phenol across the membrane.

Electron Microscopy

Scanning electron microscopy (SEM) and transmission electron microscopy (TEM) were used to image the carbon nanotubes prepared within the pores of the alumina template membrane. This was accomplished by first dissolving away the alumina by immersion (for 12 hours) in 49% HF. The HF was removed by pipette leaving the liberated nanotubes (connected together by the carbon surface films, Figure 2-2A), which were rinsed with methanol and then suspended in methanol. This suspension was then

ultrasonicated for 20 min. It is important to point out that removal of the template membrane in this way was only done for the SEM and TEM images. All permeation studies were done with the carbon nanotubes still embedded within the pores of the alumina template.

For the preparation of SEM samples a drop of the ultrasonicated membrane suspension was applied to a copper foil adhered to a SEM stub and the solvent was allowed to evaporate. Gold was sputtered onto the sample in order to improve electrical conductivity. Images were obtained using a JEOL 6335F field emission gun microscope. For TEM imaging a drop of the suspension was applied to a Carbon Type A TEM grid. The carbon nanotubes adhered well to the grid and were easily imaged using a JEOL 2000 microscope.

Results and Discussion

Electron Microscopy

Figure 2-2A shows a cross-sectional image of the CVD carbon nanotubes after dissolution of the alumina template. A parallel array of nanotubes is obtained because the tubes are connected together by the carbon surface film that can be seen at the top of the image. While it is not evident from this image, this carbon surface film does not block the mouths of the nanotubes. The outside diameter of the nanotubes (~300 nm) is larger than the nominal pore diameter of the template. Our SEM and TEM images indicate that this is because the pores are, in fact, larger than the nominal diameter for most of the thickness of the membrane but branch at one face of the membrane into smaller (diameter ~200 nm) pores. This branching can be seen in the TEM image shown in Figure 2-2B. Branching results from the voltage reduction technique used during the final step of the electrochemical process used to prepare these alumina membranes.[128]

Figure 2-2B shows a TEM montage image of individual carbon nanotubes that had become separated from the carbon surface films during ultrasonication of the nanotube suspension. The branched ends of the nanotubes discussed above are clearly seen in this image. This image also shows that the tubes have a consistent wall thickness down their entire length; a wall thickness value of ~40 nm was obtained from such images.

XPS

Survey scans (not shown) indicate that only oxygen and carbon are present on the surface of the CNMs. While these spectra were obtained with the underlying alumina membrane still intact, there is no observable signal for Al because the carbon layer is too thick (~40 nm). This allows us to assign the oxygen signal to oxygen-containing functional groups on the carbon surface. The high-resolution C 1s spectra may be fitted to five peaks (Figure 3-2). The top panel of Figure 3-2 shows the fit envelope overlaid on the original spectrum; the bottom panel shows the peak contributions to the fitted envelope. The binding energies for the five peaks are as follows: 283.9±0.4 eV, 285.0 eV (reference peak), 286.3±0.5 eV, 287.8±0.5 eV and 289.9±0.4 eV, where the averages are for 6 values, and the uncertainties are the unbiased standard deviations.

Ramm et al. have recently used XPS to characterize the surface composition of plasma-deposited amorphous carbon films.[138] They assign the two lowest binding-energy peaks to graphitic (284 eV) and amorphous (285 eV) carbon present at the surface of the sample. The predominance of the 285 eV peak indicates that, in agreement with prior results, these carbon nanotube are amorphous.[55] They can, however, be converted to highly ordered graphite via a Ni catalysis method.[55] The three higher binding-energy peaks are due to oxygen-containing surface functional groups. These three peaks may be assigned as follows: 286.3±0.5 eV - alcohol or phenolic hydroxyl, ether; 287.8±0.5 eV –

aldehyde, ketone; 289.9±0.4 eV - carboxylic acid, ester, carboxylic acid anhydride.[139] It is well known that air-oxidized carbon surfaces contain carboxylic acid groups.[133-135] and presumably anhydride would hydrolyze to the acid upon exposure to water. These sites contribute to the intensity of the 289.9 eV peak. However, XPS alone cannot distinguish between –COOH and the contribution from ester sites. As we will see, EOF measurements allow for a determination of both the surface density of acidic sites and the surface pK_a.

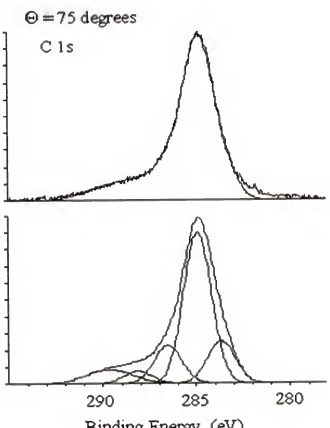

Figure 3-2. High resolution C 1s XPS spectrum showing the experimental spectrum, the fitted envelope, and the individual peaks for the fit.

Effect of Magnitude of the Applied Current on Permeate (Phenol) Flux

Figure 3-3 shows a plot of micromoles of phenol transported across the carbon nanotube membrane at various values of applied current density. This plot consists of

five linear segments, and the slope of each segment is the flux of phenol (N_J) at that applied current density (Table 3-1). The first linear segment in Figure 3-3 (0 to 8.5 min) was obtained with no applied current, and the flux in this case is simply the diffusive flux of phenol, N_{diff}, from the feed across the membrane and into the permeate. The second linear segment (9 to 14.5 min) was obtained with an applied current density, J_{app} = -7.2 mA cm^{-2}. The flux of phenol across the membrane was observed to decrease, indicating EOF in the opposite direction of the diffusive flux (EOF from permeate solution to feed solution). This is confirmed by data in the third linear segment (15 to 20.5 min), which were obtained with J_{app} = +7.2 mA cm^{-2}; now the net flux is higher than the diffusive flux (Table 3-1) indicating EOF in the direction of diffusive transport. The final two linear segments were obtained at higher positive and negative applied current densities, and further enhancement and diminution, respectively, in the flux is observed.

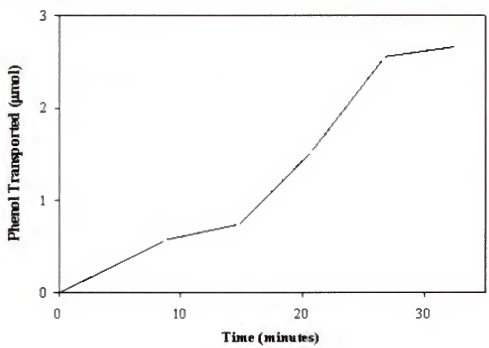

Figure 3-3. Micromoles of phenol transported vs. time at various values of applied current density (see Table 3-1 for current density values).

Table 3-1: Effect of applied current density on the flux, enhancement factor and electroosmotic velocity in the carbon nanotube membrane

J_{app} mA/cm^2	Flux nmol/(min·cm^2) [a]	E	υ_{eo} μm/s
-10.1	25.8	.280	-35.0
-7.2	39.3	.426	-24.5
0.00	92.1	1.000	0.0
+7.2	187.1	2.030	26.3
+10.1	237.9	2.581	37.6

[a]The geometric area of the membrane (0.713 cm^2) was used.

Calculation of the Electroosmotic Velocity

In the presence of the applied transmembrane current, the steady-state flux of permeant across a membrane is described by the Nernst-Plank equation[140]

$$N_J = -D\,[\partial C(x)/\partial x] - zF(RT)^{-1}\,DC\,[\partial\phi(x)/\partial x] \pm C\upsilon_{eo} \qquad (3\text{-}1)$$

where D, C and z are the diffusion coefficient, concentration and charge of the permeate molecule, respectively, $\partial C(x)/\partial x$ is the concentration gradient in the x direction across the membrane, $\partial\phi(x)/\partial x$ is the potential gradient in the electrolyte within the nanotubes, and υ_{eo} is the electroosmotic velocity. The three terms in Equation 3-1 describe the diffusive, migrational and EOF-convective transport processes, respectively. Because phenol is a neutral molecule at the pH used here, Equation 3-1 simplifies to

$$N_J = -D\,[\partial C(x)/\partial x] + C\upsilon_{eo} \qquad (3\text{-}2)$$

When $J_{app} = 0$, only the first term in Equation 3-2 is operative and the flux is the diffusive flux, N_{diff}.

The experimental flux data in Table 3-1 can be used to calculate a parameter called the enhancement factor, E, which can then be used to calculate the electroosmotic velocity.[140] E is given by,

$$E = N_J/N_{diff} \qquad (3\text{-}3)$$

i.e., the ratio of the flux in the presence of an applied current to the flux at $J_{app} = 0$. E values for the data in Figure 3-3 are presented in Table 3-1. When a positive current is applied, E is greater than unity, indicating, again, EOF in the direction of the diffusional flux. Analogous results were obtained by Bath et al. for Nafion membranes, where EOF is due to the polymer's fixed sulfonate sites.[112] This indicates that, as would be expected for air-treated carbon, the pore walls on the carbon nanotubes have fixed negatively charged sites.[133-135]

Following Srinivasan and Higuchi,[140] the peclet number (Pe) can be calculated from E via

$$E = Pe/(1-e^{-Pe}) \qquad (3\text{-}4)$$

Pe can then be used to calculate υ_{eo} using[140]

$$\upsilon_{eo} = Pe\ D / l \qquad (3\text{-}5)$$

where l is the thickness of the membrane. Because the inside diameter of the carbon nanotubes (~120 nm) is ~500 times larger than the diameter of phenol, hindered diffusion[141] does not occur in these tubes, and the bulk solution diffusion coefficient can be used in Equation 3-5. The diffusion coefficient and the membrane thickness (0.006 cm) give the υ_{eo} data shown in the last column in Table 3-1. As would be expected,

current densities of the same magnitude but opposite sign give υ_{eo} values of approximately the same magnitude but opposite sign.

Effect of Applied Current Density on υ_{eo}

Phenol transport data like those shown in Figure 3-3 were obtained for 16 different J_{app} values between +19.3 and –19.3 mA cm^{-2}. Figure 3-4A shows the corresponding flux vs. J_{app} data. As would be expected from the above results, flux increases with J_{app} for positive currents, indicating the increasing importance of EOF to the transport of permeate across the membrane. At sufficiently negative J_{app} values, the net flux asymptotically approaches zero. In this case, EOF from the permeate half-cell to the feed half-cell is negating the diffusive flux from feed to permeate.[112]

The Helmholtz-Smoluchowski equation[142] describes the relationship between the electroosmotic velocity and the linear electric field gradient (E(x), V cm^{-1}) across the membrane

$$\upsilon_{eo} = -\varepsilon\zeta E(x) / \eta \qquad (3\text{-}6)$$

where ε and η are the permittivity and viscosity of the solution within the nanotubes, respectively, and ζ is the zeta potential of the tube walls. Substituting the product of the applied current density and the resistivity of the electrolyte within the nanotubes, ρ, for the E(x) in Equation 3-6 gives

$$\upsilon_{eo} = -\varepsilon\zeta J_{app}\rho / \eta \qquad (3\text{-}7)$$

which shows that υ_{eo} is linearly related to the applied current density. Equations 3-4 and 3-5 were used to calculate υ_{eo} from the flux data in Figure 3-4A. Figure 3-4B shows a plot of υ_{eo} vs. current density; in agreement with Equation 3-7, a linear relationship is obtained. (Some deviation is observed at the highest negative J_{app} values. This is

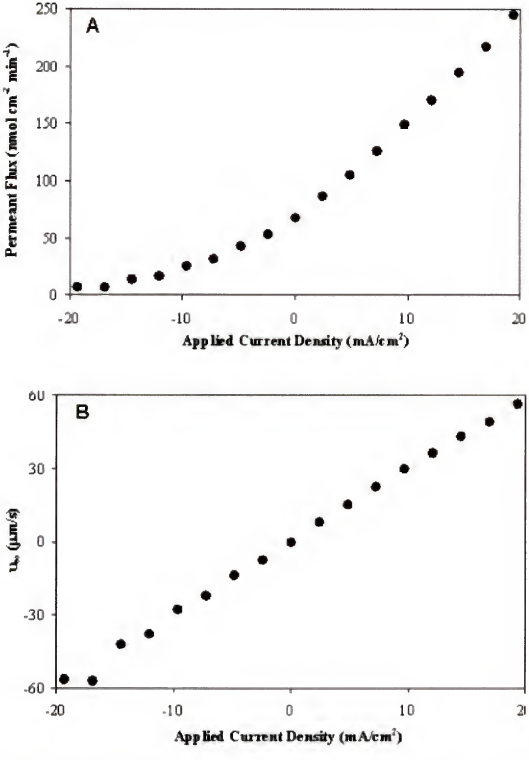

Figure 3-4. Effect of applied current density on CNM transport phenomenon. (A) Plot of phenol flux vs. applied current density. (B) Plot of electroosmotic flow velocity vs. applied current density.

because the flux is nearly zero at such large negative J_{app}'s, making the error in the measurement large.).

According to Equation 3-7, the slope of the υ_{eo} vs. J_{app} plot in Figure 3-4B is $-\varepsilon\zeta\rho/\eta$. Using the known values for the permittivity and viscosity of water (6.95×10^{-10} $C^2\ J^{-1}\ m^{-1}$ and 0.890 cP, respectively)[143] and the measured resistivity of the electrolyte (2.23 kΩ cm), the slope can be used to calculate the zeta potential for the CNM. A value of ζ = -17.3 mV was obtained from these data. Bismark et al., obtained similar zeta potential values for carbon fibers,[134] and Garcia et al., obtained somewhat larger zeta potential values (~-45 mV) after grinding such carbon fibers.[135]

It should be noted that Equations 3-6 and 3-7 are based on the assumption that the thickness of the double layer at the pore wall is much smaller than the pore radius. Because the double layer at this electrolyte concentration is less than 3 nm in thickness,[142] this is clearly a valid assumption. Finally, due to the relative thinness of the double layer and because the measured zeta potential is relatively low, deviations due to surface conductance, or changes in the permittivity, and viscosity within the nanotubes are negligible.[144,145] Thus, it is reasonable to use the resistivity, permittivity, and viscosity of the bulk solution in the zeta potential calculation.

Effect of Ionic Strength of the Electrolyte on υ_{eo}

Phenol transport data were obtained at applied current densities of +19.7 and –19.7 mA/cm^2 in solutions with ionic strength varying from 0.01 M to 0.50 M (Figure 3-5). The pH of the electrolyte was maintained at 7.2. Transport data for the case $J_{app} = 0$ were also obtained over this electrolyte concentration range. No change in the diffusional flux was observed (<3% relative standard deviation), indicating that the diffusion coefficient

for phenol does not vary with electrolyte concentration over this concentration range. Figure 3-5 shows plots of υ_{eo} vs. ionic strength obtained from the transport data. The general trend - that the absolute value of υ_{eo} decreases with increasing ionic strength - is as expected.

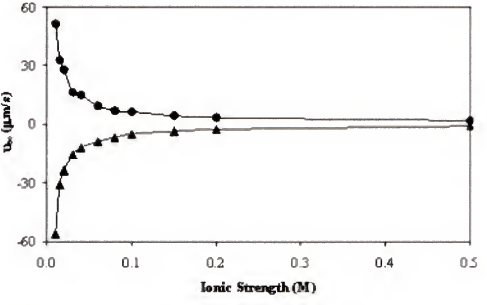

Figure 3-5. Plots of electroosmotic flow velocity vs. the ionic strength of the permeate and feed solutions. Applied current densities were ▲ –19.7 mA cm^{-2} and ● +19.7 mA cm^{-2}.

Returning to Equation 3-7, we see that υ_{eo} is directly proportional to the zeta potential, which is related to the Debye length, κ^{-1}, (the effective thickness of the electrical double layer) by[146]

$$\zeta = 2kT/ze \sinh^{-1} (\sigma\kappa^{-1}ze/(2\varepsilon kT)) \qquad (3\text{-}8)$$

where k is the Boltzmann constant, T is temperature, e is the elementary charge, and σ is the surface charge density at the plane of shear between the nanotube wall and the electrolyte. For the zeta potential and Debye length ranges investigated here Equation 3-8 simplifies to

$$\zeta = \sigma\kappa^{-1}/\varepsilon \qquad (3\text{-}9)$$

For a symmetrical electrolyte, κ^{-1} is related to the concentration of the electrolyte via[142]

$$\kappa^{-1} = 9.61\text{x}10^{-9}(z^2c)^{-1/2} \qquad (3\text{-}10)$$

Equation 3-10 shows that the double layer thickness decreases with increasing ionic strength of the electrolyte, which means that the zeta potential decreases with increasing ionic strength (Equation 3-9). This, in turn, causes $|\upsilon_{eo}|$ to decrease with increasing ionic strength (Equation 3-7), which is the experimentally observed trend in Figure 3-5.

A second factor contributes to the observed decrease in $|\upsilon_{eo}|$ with increasing ionic strength. Equation 3-7 shows that υ_{eo} is also proportional to the resistivity of the electrolyte, ρ, which is inversely proportional to the number of charge-carrying ions in the solution. Hence, ρ decreases with increasing ionic strength of the electrolyte, and Equation 3-7 predicts that this would also contribute to the observed decrease in υ_{eo} with increasing ionic strength (Figure 3-5).

If it is assumed that κ^{-1} decreases with ionic strength (μ) as $\kappa^{-1} \propto \mu^{-1/2}$ (Equation 3-10) and that ρ decreases with μ as $\rho \propto \mu^{-1}$, we would predict that υ_{eo} would decrease with μ via $\upsilon_{eo} \propto \mu^{-3/2}$. The experimental data (Figure 3-5) were fit to the relationships $\upsilon_{eo} \propto \mu^{-0.9}$ ($R^2 = 0.993$) for the positive current density and $\upsilon_{eo} \propto -\mu^{-1.0}$ ($R^2 = 0.997$) for the negative current density. Hence, the experimental falloff of υ_{eo} with increasing μ is less than the predicted value.

Another factor needs to be considered. As shown in Equation 3-9, the zeta potential is also directly proportional to the charge density. The charge density can be divided into two general categories – covalently-bound charge and adsorbed charge. We discuss the effect of the quantity of covalently-bound charge on υ_{eo} in the following

section. It is possible that over the very large ionic strength range investigated in Figure 3-5, there is a significant change in the quantity of adsorbed charge from the electrolyte. Adsorbed charge would primarily come from the anions of the electrolyte, and this adsorbed negative charge would increase with increasing μ. This would cause both the zeta potential and υ_{eo} to increase with increasing μ. Since this is the opposite trend as the $\kappa^{-1} \propto \mu^{-1/2}$ and the $\rho \propto \mu^{-1}$ dependences discussed above, this would make the net decrease in υ_{eo} with increasing μ less extreme than the predicted $\mu^{-3/2}$ dependence, and this is what is observed experimentally.

Finally, at the highest ionic strength used in Figure 3-5, both the negative and positive electroosmotic velocities decrease to near zero. This shows that the effect of double layer compression on the zeta potential (that causes υ_{eo} to decrease with increasing ionic strength) dominates any effect of increasing adsorbed negative charge at high ionic strengths.

Effect of Solution pH on υ_{eo}

Phenol transport data were obtained at applied current densities of positive and negative 24.9 mA cm^{-2} from solutions that were 10 mM in NaCl and 0.5 mM in phosphate, with the pH adjusted to values between 3 and 8. The NaCl served to maintain the ionic strength at a constant value. The υ_{eo} vs. solution pH data are shown in Figure 3-6A. In general, the expected trend for surface acidic sites is observed; i.e., υ_{eo} is high at high pH values, where the sites are deprotonated, and goes to zero at lower pH values where the sites are protonated. There are, however, two features of the data in Figure 3-6A that are unexpected.

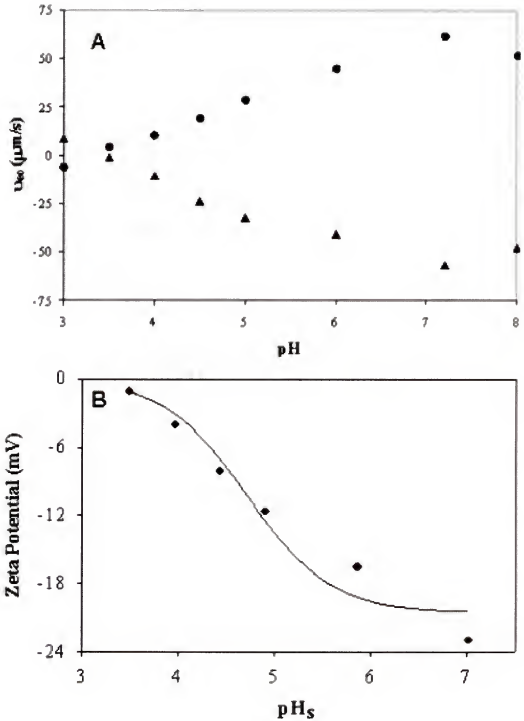

Figure 3-6. Effect of solution pH on EOF and CNM zeta potential. (A) Plots of electroosmotic flow velocity vs. pH. Applied current densities were ▲ –24.9 mA cm^{-2} and ● +24.9 mA cm^{-2}. (B) Plot of Zeta potential of the CNM vs. surface pH (Equation 3-11). The points are the experimental data the curve is the best fit to Equation 3-13.

First, while υ_{eo} goes to zero at pH ~3.5, at lower pH the flow resumes again, but in the opposite direction. This indicates that positive sites are introduced by protonation of some very weakly basic surface functional group. Such protonatable carbon sites have been known for some time and have been attributed to two chemical features of the carbon - pyrone-like structures and basal-plane sites that act as Lewis bases.[147] These protonatable carbon sites have also been observed in zeta potential measurements of carbon fibers.[134,135] The presence of these sites makes the EOF characteristics of the carbon nanotubes quite interesting because the direction of EOF can be switched by controlling the pH of the contacting solution phase.

The second unexpected feature of the data in Figure 3-6A is that $|\upsilon_{eo}|$ at pH = 8.0 is lower than at pH = 7.2. While it is tempting to attribute this to experimental error, it was observed at all current densities studied and with both positive and negative currents. This is unexpected because the fraction of the deprotonated form of a monoprotic weak acid (α_1) goes to a maximum (α_1= 1) at some high pH and does not change at higher pH values. Hence, the plots of υ_{eo} vs. pH would be expected to become flat at high pH. The unexpected decrease in $|\upsilon_{eo}|$ suggests that anionic surface charge density decreases from pH = 7.2 to pH = 8.0. As discussed above, it is possible that adsorbed phosphate contributes to the surface charge on the carbon nanotubes. One plausible explanation is that at pH = 8.0 adsorbed HPO_4^{2-} is displaced by OH^-, resulting in a net decrease in the negative surface charge density.

The data in Figure 3-6A can be used to determine both the number density and pK_a of the surface acidic sites on the carbon nanotube membranes.[146] The Boltzmann

equation is first used to calculate the surface hydronium ion concentration ($[H^+]_s$) from the bulk solution hydronium ion concentration ($[H^+]_o$).

$$[H^+]_s = [H^+]_o \exp(-e\zeta/2kT) \qquad (3\text{-}11)$$

The requisite zeta potential values at each pH are obtained as before from the υ_{co} data (Figure 3-7A). Following Jimbo et al.,[146] the surface charge density is related to the number density of acidic sites (N_a) and the surface pK_a via

$$\sigma = -[(eN_a) / (1 + 10^{pK_a - pH_s})] \qquad (3\text{-}12)$$

Equation 3-9 can be solved for σ and set equal to Equation 3-12. Solving for the zeta potential gives

$$\zeta = -[(eN_a) / (1 + 10^{pK_a - pH_s})] (\kappa^{-1}/\varepsilon) \qquad (3\text{-}13)$$

Figure 3-6B shows a plot of ζ vs. pH obtained from the data in Figure 3-7A, omitting the highest and lowest pH values where unusual effects (*vide supra*) were observed. The points are the experimental data, the curve is the result of a nonlinear least squares regression fit of Equation 3-13 to the experimental data using the surface pK_a and N_a as adjustable parameters. The best fit ($R^2 = 0.95$) was obtained for $pK_a = 4.7$ and $N_a = 0.03$ acidic sites per nm^2.

The surface pK_a value obtained is typical of that for an alkyl carboxylic acid (e.g., acetic acid) dissolved in aqueous solution. However, it is often the case that pK_a values for surface-bound species differ from those obtained when the corresponding molecule is dissolved in an aqueous solution. For example, the pK_as for p-aminobenzoic acid[148] and 4-carboxyphenyl[149] immobilized on glassy carbon electrode surfaces were measured to be 3.0 and 2.8, respectively. These values are significantly different from the pK_as for the same molecules dissolved in aqueous solution – p-aminobenzoic acid = 4.6 and benzoic

acid = 4.2. For this reason, while the most likely assignment for the surface acidic sites is carboxylic acid, we cannot unambiguously make this assignment at this time. A less likely alternative would be to posit a surface phenolic site whose surface pK_a has been dramatically shifted from the typical solution value. One potential source for discrepancies between surface and free-solution pK_a values is electrostatic interactions between the surface-bound sites. The site density of 0.03 per nm^2 indicates that the sites are on average 3 nm apart.[150] This is comparable to the double-layer thickness at the ionic strength used to obtain the data in Figure 3-6. Hence, electrostatic interactions between surface acidic sites should not be significant.

The Effect of Cationic Surfactant on υ_{eo}

Addition of cationic surfactants is a simple, rapid, and reproducible method of reversing the surface charge of an anionic capillary.[132,151] Small amounts of surfactant, at concentrations as small as 10% the critical micellar concentration (cmc), form bilayers at the capillary walls (Figure 3-7). This dynamic method results in reversal of EOF, and has been shown to substantially shorten analysis time and improve resolution in capillary electrophoresis-based separation of anions.[151]

Figure 3-8 shows plots of υ_{eo} vs. applied current density for a CNM before and after making the permeate cell solutions 0.25 mM in the cationic surfactant hexadecyltrimethylammonium chloride (HTAC). Considering the as-synthesized membrane first, we see the expected change from positive electroosmotic flow at the positive applied current, to zero flow at no applied current, to negative EOF at negative applied current (Table 3-1). The measured slope of the line corresponds to a zeta potential of -16.9 mV for the as-synthesized membrane (Figure 3-8).

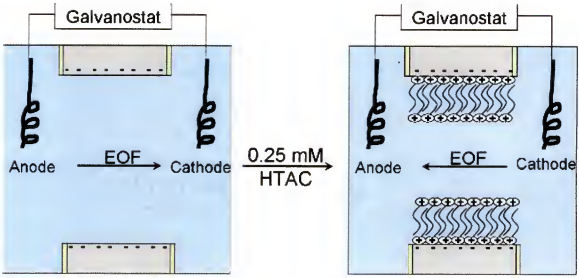

Figure 3-7. Cationic surfactant bilayer method of dynamic electroosmotic flow reversal (illustration).

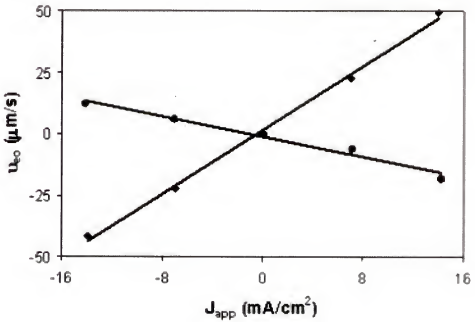

Figure 3-8. Reversal of EOF with cationic surfactant. Plots of electroosmotic velocity vs. applied current density for ♦ as-synthesized membrane and ● CN/HTAC membrane.

For the CN/HTAC membrane, positive EOF is observed at negative applied currents and negative EOF is observed at positive applied currents (Figure 3-8). This indicates that a surfactant bilayer has indeed formed at the charged nanotube surface and the zeta potential and thus surface charge is now positive (Figure 3-7). The zeta potential for the surfactant bilayer nanotubes was determined to be +5.1 mV. Note, however, that the magnitude of the zeta potential for the membrane is not as great as for the bilayer-free CNM. While this might be due to a lower surface charge density for the CN/HTAC membrane, other factors contributing to zeta potential (Equation 3-8) must also be considered. For the bilayer-free membrane, the solution-side of the double layer contains monovalent Na^+ ions. In contrast for the CN/HTAC membrane, the double layer contains a mixture of monovalent $H_2PO_4^-$ and divalent HPO_4^{2-} ions. The presence of the divalent ions (which are electrostatically preferred over the monovalent) will compress the double layer relative to the case where only monovalent ions are present.[152] As a result, at any surface charge density value, the double layer will be thinner when multivalent ions are present. This will cause the zeta potential to be lower and υ_{eo} to be smaller than in the monovalent case. This factor undoubtedly contributes to the smaller slope and ζ observed for the CN/HTAC membrane (Figure 3-8).

Conclusions

EOF was driven across template-prepared carbon nanotube membranes and the rate and direction of flow was controlled by changing the magnitude and the sign of the trans-membrane current. The direction of EOF was also switched by varying the pH of the contacting solution phase. All of these pH-induced changes in EOF were reversible. This means, for example, that returning a membrane that had been exposed to pH = 3.5

buffer, where no EOF was observed (Figure 3-6A), to pH = 7.2 buffer, restored the flow. Cationic surfactants have been used to assemble cationic bilayers at the anionic nanotube walls, thus changing the charge of the membrane from negative to positive. This provides a route for dynamically reversing the direction of EOF.

There are other ways to affect the rate and direction of EOF in such membranes. We have shown with gold nanotube membranes that conductive membranes can be used as electrodes to modulate transport.[73,74] In addition, we have shown that carbon nanotube membranes can also be used as electrodes.[32,33,85] In Chapter 4 we will investigate the use of electrochemical methods to modify and modulate the EOF characteristics of CNMs. This ability to combine electrochemical capabilities with an EOF device is unique to template-prepared CNMs.

CHAPTER 4
TAILORING ELECTROKINETIC PROPERTIES OF CARBON NANOTUBE MEMBRANE ELECTRODES

Introduction

Template synthesis, as a general method for preparing nanomaterials, was significantly advanced in the Martin laboratory in late 1980s and early 1990s.[50,86,87] However, this method has its roots as far back as 1970 in work by Possin where metal nanowires were prepared in track-etch mica.[88] Many other types of nanostructured materials have been prepared with this method including conductive and insulating polymers, semiconductors, carbons, sol-gels, and composite structures.[49,50] The key feature of template synthesis is the unprecedented growth control that can be achieved in preparing large numbers of homogenous nanotubes or nanowires.

One very interesting aspect of nanotubes prepared by the template-method is that the tubes can be left intact within the template resulting in a "nanotube membrane".[92] In these membranes each nanotube serves as a pore. For instance, gold nanotube membranes have been prepared and studied extensively in the Martin laboratory.[73,74,95,127] These membranes are prepared by electroless gold deposition in polymeric track-etched membranes.[96] Gold nanotube membranes have proven accommodating to a number of novel applications in separations and as sensors.[100,153] Since gold is electronically conductive, gold nanotube membranes have been set up as working electrodes and electrochemically charged in order to electromodulate transport across the membrane.[73,74,127] In this configuration each tube in the membrane approximates a

narrow capillary in which the surface charge is controlled potentionmetrically. Therefore, these membrane/electrodes allow selective transport of cations or anions purely as a function of electrode potential. In other work, gold nanotube membranes have themselves been used as templates for the preparation of concentric Au-Polymer composite nanotubes by electropolymerization.[154]

Analogous to the gold nanotube membrane are membranes which contain a dense array of monodisperse, aligned carbon nanotubes serving as pores.[33,53] As described in Chapter 2, disordered graphitic carbon nanotubes can be grown in nanoporous, anodic aluminum oxide template membranes by controlled chemical vapor deposition (CVD) of carbon. The template-prepared carbon nanotubes are an excellent membrane material as their inside-diameters are easily tailored over a wide range. We have prepared carbon nanotube membranes (CNMs) with nanotube i.d.s ranging from ~10 nm to 200 nm (Chapter 2). However, carbon nanotubes with even smaller inner diamters should be achievable, as have been done with gold nanotubes.[95] In addition, CNMs are electronically conductive which allows them to be used as electrodes in a manner similar to the Au membrane electrodes.[32,33,53,85]

More recently we have become interested in electroosmotic flow (EOF) and have used it to modulate molecular delivery across CNMs (Chapter 3).[53,155] We have shown that we can control EOF using trans-membrane current, concentration and pH of electrolyte solution, and surface chemistry. Control of EOF is very important in many separations techniques including capillary electrophoresis and electrochromatography, lab-on-a-chip electrophoresis, and a number of membrane-based methods. However, EOF control is of particular importance as the method of choice for manipulating samples

and reagents in the majority of microfluidic devices.[115,121] In addition, the interplay and control of EOF between nanoporous membranes and microchannels is of special interest in complex nano/microfluidic systems.[122,123]

According to Helmholtz-Smoluchowski theory,[53] dynamic control of EOF velocity (υ_{eo}) is easily accomplished by adjusting the magnitude and polarity of the flow-driving electric field; but this parameter likewise impacts the electrophoretic transport of ions and charge particles in solution. However, υ_{eo} scales directly with zeta potential (ζ) as well. ζ is characteristic of the electric field induced by a charged surface in solution and scales with surface charge. Thus, υ_{eo} scales directly with surface charge. By dynamically adjusting surface charge (i.e. ζ) on a channel, capillary, or pore wall, electroosmotic flow can, in principal, be decoupled from electrophoresis. In other words, transport due to EOF and electrophoresis can be controlled independently of each other. Classic methods of dynamic EOF control are chemical, such as pH adjustment of electrolyte,[53] surfactant additives,[132] and multilayered polyelectrolyte coatings.[156] Other non-chemical methodologies include coating microchannels with semiconductive TiO2, which when irradiated with UV light, changes surface charge and thus EOF.[157] Finally, field effect control has been studied by several groups where radial electric fields are applied across the walls of a capillary[120,158] or microchannel.[121] The applied radial field enhances or diminishes ζ and has been used to modulate EOF and even reverse it at pHs near the point of zero charge (pzc).

In the work reported in this chapter, we take advantage of the electronic conductivity of carbon nanotubes to modify the inner walls of the tubes. There are many reasons for modifying the surfaces of an EOF device.[159,160] For instance, one common

goal for such modifications is to eliminate, incorporate, or enhance certain analyte-surface interactions. Our goal for modifying CNMs was to alter and control the EOF properties of the membranes. For example, in one set of experiments we used an electrochemical derivatization method to attach carboxylate groups to the nanotube walls.[148,161,162] This enhances the native anionic surface charge, resulting in a corresponding increase in the EOF rate. Electrochemical derivatization was also used to attach cationic ammonium sites to the nanotube walls to yield CNMs that show EOF in the opposite direction of the as-synthesized and carboxylated membranes.

We have also used electrochemical polymerization methods to prepare carbon nanotube-polymer composite membranes.[124,125] In membranes modified with polyphenylene oxide (PPO), EOF was passivated although the nanotubes remained open allowing diffusion and electrophoretic migration. In other CNMs, modified with the redox-active polymer poly(vinyl ferrocene) (PVFc), we demonstrated a new system of dynamic EOF control. We reasoned that surface charge of a nanotube modified with a redox-active species, such as ferrocene, could be controlled based on red/ox state. Thus, EOF could be electrochemically redox-modulated in such a membrane (Figure 4-1). This is a new method of dynamic EOF control that has never been demonstrated before.

Expermimental

Materials

Whatman Anodisc microporous alumina filters were used as the template membranes. Argon, nitrogen, phenol, $AgNO_3$, p-aminobenzoic acid, 2-(4-aminophenyl) ethylamine, 2,6-dimethylphenol, potassium chloride, potassium ferric-cyanide, vinylferrocene, and tetrabutylammonium perchlorate were used as received. A 30:70 (v/v) mixture of ethylene and He was used for CVD synthesis of the carbon nanotubes.

Absolute ethanol and acetonitrile were dried over 3Å molecular sieves. $LiClO_4$ was dried at 90 °C. Purified water was prepared by passing house-distilled water through a Millipore Milli Q water purification system. Phosphate buffer solutions were prepared from monobasic sodium phosphate and adjusted to pH 7.2 with 1 M NaOH. Potassium perchlorate solutions were adjusted to pH 3.5 with 1 M $HClO_4$.

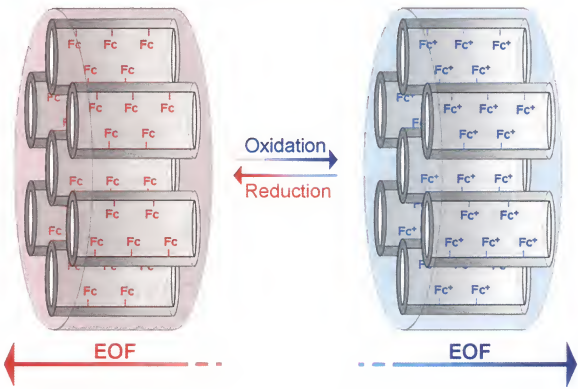

Figure 4-1. Redox-modulated electroosmotic flow in a carbon nanotube membrane modified with ferrocene (illustration).

Preparation of the Carbon Nanotube Membrane Electrodes

The CVD method used has been described previously in Chapter 2 and elsewhere.[33,53,55] The specific procedure for the membranes studied in this chapter was slightly modified from the work reported in Chapter 3. Briefly, prior to CVD synthesis, the alumina template membranes were pre-treated at 740 °C for one hour. This was done to prevent unwanted curling, and allowed synthesis of planar CNMs. The template

membrane was placed vertically in the reactor and CVD of carbon was done at 690 °C for 4.5 hours. After CVD, the Ar flow was resumed, the ethylene flow was terminated, and the CNM was allowed to anneal at the CVD temperature for 2 hours. After annealing, the furnace was turned off and allowed to cool to room temperature. The CNM was mounted in the supporting assembly (Figure 3-1A) as described in Chapter 3. CNMs prepared in this way are referred to as "as-synthesized" membranes.

Electrochemical Derivatization of Carbon Nanotubes with Primary Amines

An electrochemical derivatization scheme[148,161,162] was used to attach carboxylate groups to the nanotube walls. This method entails the electrooxidation of p-aminobenzoic acid (PABA) to a cation radical at the carbon nanotube walls. This results in the formation of a C-N bond, thus covalently attaching PABA to the tube walls. Dong et al, used a series of electrochemical experiments at glassy carbon electrodes to prove that at neutral pH values, the PABA dissociates to yield covalently bound surface carboxylate groups.[148] A similar approach was used to attach positively charged ammonium sites to the nanotube walls. This entailed electrochemical oxidation of 2-(4-aminophenyl) ethylamine (APEA) at the carbon nanotube membrane to yield covalently bound APEA. At neutral pH values, the free (not bound to the tube wall) amine sites are protonated to the corresponding ammonium cation.

The electrochemical cell used for these derivatizations consisted of the CNM working electrode, a Ag/Ag^+ reference electrode (0.01 M $AgNO_3$ in anhydrous ethanol) and a platinum mesh counter electrode; the electrolyte solution was 0.1 M $LiClO_4$ in anhydrous ethanol which was also 3 mM in either PABA[148] or APEA. The electrochemical reaction was carried out by scanning the potential of the carbon nanotube

membrane working electrode three times between 0 and +1.2 V vs. Ag/Ag^+ (scan rate = 10 mV s^{-1}).

Growth of PPO Nanotubes Inside Carbon Nanotubes

An electropolymerization method for growing poly(2,6-dimethyl-1,4-phenylene oxide) electrode coatings was adapted to CNMs.[124] This method entails the electrooxidation of 2,6-dimethylphenolate anions to form intermediate radicals which polymerize, coating the electrode surface.[124] Defect-free PPO films are grown which, at ~50 nm in thickness, effectively block the approach of monomer to the electrode, thus halting film growth.[163]

The electropolymerization cell consisted of the CNM working electrode, a Ag/AgCl reference electrode and a Pt wire counter electrodes; the electrolye solution was anhydrous methanol, 0.05 M in 2,6-dimethylphenol and 0.3 M in NaOH. The electropolymerization of the inner PPO nanotubes was accomplished using cyclic voltammetry with six times scans between 0 V and +1.2 V (scan rate = 10 mV s^{-1}). The CN/PPO membrane was rinsed and sonicated in methanol and allowed to dry. To verify that defect-free inner PPO nanotubes had formed, cyclic voltammetry was performed at the CNM-electrode before and after PPO deposition. The 0.1 M KCl electrolyte solution was 4 mM in $K_3Fe(CN)_6$, which has been demonstrated to be impermeable in PPO films.[154,163]

Electromodification of CNMs with Poly(vinylferrocene)

Poly(vinylferrocene) (PVFc) is well known to be a stable and reversible electroactive polymer that is positively charged when oxidized but uncharged when reduced. Additionally, uniform PVFc films a few nanometers thick have been grown by electrochemical reduction of vinylferrocene on glassy carbon electrodes.[125] Such thin-

films are ideal for template synthesis and the method was adopted to grow PVFc-carbon composite nanotubes. This electropolymerization reaction is believed to entail the electrochemical reduction of the monomer to generate anionic radicals on the vinyl group.[164]

The electrochemical cell contained deoxygenated and blanketed acetonitrile solution 8 mM in vinylferrocene and 50 mM in tetrabutylammonium perchlorate. The CNM was the working electrode with Ag/AgCl as the reference electrode and Pt mesh as the counter electrode. Modification was by cyclic voltammetry beginning at 0 V and scanned 24 times from +1.0 V to -2.8 V (scan rate = 10 mV/s). The CN/PVFc membranes were well rinsed and sonicated in acetonitrile followed by rinsing with acetone and water. To eliminate any irreversibly oxidized PVFc, the reduced membranes were soaked for 24 hours in 0.1 M KCl. It is well known that in reduced form ferrocene is stable while the oxidized form (i.e. ferrocenium) will dissociate in such conditions. Otherwise, the PVF-CNMs were always stored in reduced form, in pH 3.5 KClO4 solutions, in order to minimize degradation of the ferrocene moiety.

Permeation and EOF Measurements

EOF experiments were done as described in previously published work[53] and in Chapter 3. Briefly, the permeation cell was filled with 25 mL of 5 mM phosphate buffer adjusted to pH 7.2. The feed half-cell was also 5.0 mM in the electrically neutral, chromophoric probe molecule phenol. Trans-membrane current (i.e. between the feed and permeate half-cells) induced EOF through the nanotube-pores. The υ_{eo} was determined by monitoring the transport of the probe molecule across the membrane into the permeate half-cell. Sign conventions were the same as those used before.[53]

In the case of redox modulation of EOF with CN/PVFc membranes, the solutions were 0.01 M in $KClO_4$ adjusted to pH 3.5 with $HClO_4$. The redox state of these membranes was controlled during the course of the experiments by constant potential, E_{memb}, with Ag/AgCl reference electrodes and Pt wire counter electrodes in both compartments of the permeation cell. Though the current-time plots indicate that red-ox reaction response time was ~10 s, E_{memb} was applied for 30 s. In order to avoid disruption of trans-membrane current, the potentiostat (redox-control) electrodes were disconnected before this current was applied.

Results and Discussion

EOF in Carbon Nanotube Membranes

As seen in Chapter 3, EOF has been extensively studied in CNMs.[53] In brief review, Figure 3-3 shows a plot of micromoles of phenol transported across an as-synthesized CNM at various values of applied current density. This plot consists of five linear segments, and the slope of each segment is the flux of phenol (N_J) at that applied current density (Table 3-1). The first linear segment in Figure 3-3 (0 to 8.5 min) was obtained with no applied current, and the flux in this case is simply the diffusive flux of phenol, N_{diff}, from the feed across the membrane and into the permeate. The second linear segment (9 to 14.5 min) was obtained with an applied current density, J_{app} = -7.2 mA cm^{-2}. The flux of phenol across the membrane was observed to decrease, indicating EOF in the opposite direction of the diffusive flux (EOF from permeate solution to feed solution). This is confirmed by data in the third linear segment (15 to 20.5 min), which were obtained with J_{app} = +7.2 mA cm^{-2}; now the net flux is higher than the diffusive flux (Table 3-1) indicating EOF in the direction of diffusive transport. The final two linear

segments were obtained at higher positive and negative applied current densities, and further enhancement and diminution, respectively, in the flux is observed.

Electroosmotic velocities, υ_{eo}, were determined from the flux data for each applied current density by using an integrated form of the Nernst-Plank equation, Equation 3-4.[53,140] As would be expected, current densities of the same magnitude but opposite sign give υ_{eo} values of approximately the same magnitude but opposite sign (Table 3-1). This is indicative of a net negative surface charge on the nanotube walls which was attributed to native carboxylic acid functionalities.[53]

The Effect of Electrochemical Derivatization on υ_{eo}

An interesting and unique property of the carbon nanotube membranes is that they are electronically conductive and, thus, can be used as electrodes in electrochemical experiments.[32,33,85] This has allowed us to tailor the electrokinetic properties of the CNMs by electrochemically derivatizing the carbon nanotube walls to augment or change the fixed surface charge.

Figure 4-2 shows a plot of υ_{eo} vs. applied current density for an as-synthesized carbon nanotube membrane and for membranes that had been electrochemically derivatized with either 2-(4-aminophenyl) ethylamine (APEA) or p-aminobenzoic acid (PABA).[148] Each data set was determined from EOF-modulated permeation experiments similar to Figure 3-3. The pH = 7.2 buffer used was such that the carboxylic acid surface derivatives were deprotonated (anionic) and the amine surface derivatives were protonated (cationic).

The relationship between EOF and applied current density is described mathematically by the Helmholtz-Smoluchowski equation,[53]

$$\upsilon_{eo} = -\varepsilon\zeta J_{app}\rho / \eta \qquad (4\text{-}1)$$

where ε and η are the permittivity and viscosity of the solution within the nanotubes, respectively, and ζ is the zeta potential of the tube walls. This tells us that the relationship between υ_{eo} and J_{app} is linear, the slope of which corresponds to ζ. Considering the as-synthesized membrane first, we see the expected linear change from positive electroosmotic flow at the positive applied current, to zero flow at no applied current, to negative EOF at negative applied current (Figure 4-2). The measured slope of the line corresponds to a zeta potential of -20.8 mV for the as-synthesized membrane (Equation 4-1).

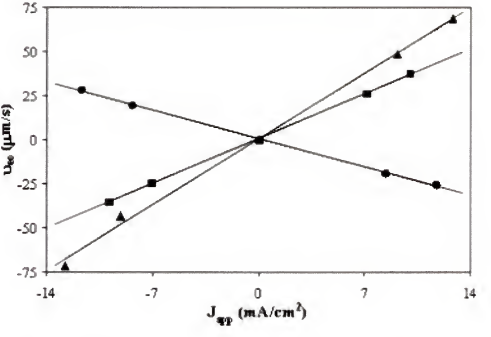

Figure 4-2. Plots of electroosmotic velocity vs. applied current density for derivatized CNMs. ▲ PABA-derivatized membrane, ■ as-synthesized membrane, ● APEA-derivatized membrane.

The same trend is observed for the PABA-derivatized membrane, but the slope of the υ_{eo} vs. applied current density line is steeper and corresponds to ζ = -30.6 mV

(Figure 4-2). This indicates that there is greater negative surface charge density after derivatization of the CNM with PABA, which was the anticipated result.

For the AEPA-derivatized membrane, positive EOF is observed at negative applied currents and negative EOF is observed at positive applied currents (Figure 4-2). This indicates that the zeta potential and thus surface charge is now positive, again the anticipated result. The zeta potential for the AEPA-derivatized membrane was determined to be +13.2 mV.

Note, however, that the magnitude of the zeta potential for the AEPA-derivatized membrane is not as great as for either the underivatized or the PABA-derivatized membranes. While this might be due to a lower surface charge density for the AEPA-derivatized membrane, other factors contributing to zeta potential (Equation 3-8) must also be considered. For the as-synthesized and PABA-derivatized membranes, the solution-side of the double layer predominantly contains monovalent Na^+ cations. In contrast for the AEPA-derivatized membrane, the double layer predominantly contains a mixture of monovalent $H_2PO_4^-$ and divalent HPO_4^{2-} anions. The presence of the divalent anions (which are electrostatically preferred over the monovalent anions) will compress the double layer relative to the case where only monovalent ions are present.[152] As a result, at any surface charge density value, the double layer will be thinner when multivalent ions are present. This will cause the zeta potential to be lower and υ_{eo} to be smaller than in the monovalent case (Equation 3-8 and 4-1). This factor undoubtedly contributes to the smaller slope and ζ observed for the AEPA-derivatized membrane (Figure 4-2).

EOF Passivation in CN/PPO Membranes

We have prepared carbon nanotube / poly(phenylene oxide) membranes (CN/PPO) by electropolymerization of 2,6-dimethylphenol on CNMs.[124] Figure 4-3A shows the six electropolymerization scans. As the PPO film grows within the nanotubes the magnitude of current observed with each scan decreases. This is indicative of electrochemical passivation of the carbon nanotube electrodes; as the PPO nanotubes thicken it becomes more difficult for the monomer species to reach the electrode surface and thus current decreases. In order to verify that defect free PPO nanotubes had formed, we did cyclic voltammetry experiments before and after the modification (Figure 4-3B). Clearly the as-synthesized CNM is electroactive as the characteristic $Fe(CN)_6^{3-}$ redox waves are present. However, after growth of PPO nanotubes, $Fe(CN)_6^{3-}$ redox waves are not observed indicating that the inner PPO nanotubes have completely covered the carbon nanotube electroactive surfaces.

Figure 4-4 shows a plot of micromoles of phenol transported across the CN/PPO membrane at various values of applied current density. Diffusive flux across the CN/PPO membrane was 42 nmol/(min·cm^2), which, not surprisingly, is less than half of what was observed for as-synthesized CNMs (Table 3-1). Undoubtedly, this drop in flux is due to the presence of PPO partially closing the nanotubes. When current was applied there was minute flux increases observed. These very small flux increases were independent of current direction indicating that they are not related to EOF. They may be due to very small amounts of phenol being incorporated into the hydration spheres of the migrating electrolyte ions. This result is in stark contrast to similar experiments with unmodified CNMs (Figure 3-3) in which very large changes in flux occurred. This clearly indicates that EOF does not occur at a significant level in the CN/PPO membrane.

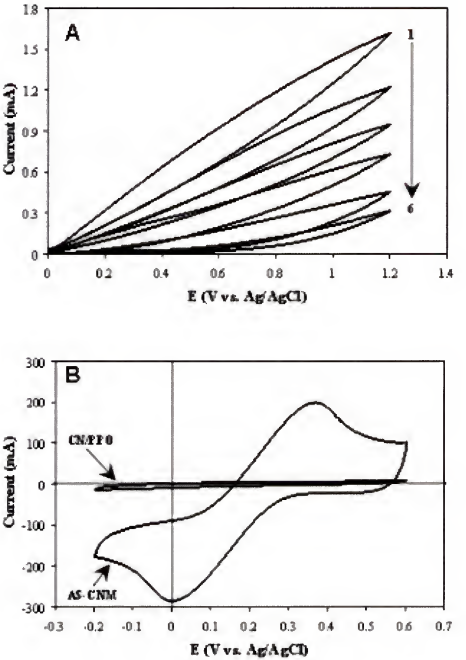

Figure 4-3. Electrochemical synthesis and characterization of CN/PPO membrane electrode (cyclyic votammograms). (A) Cyclic voltammograms for the electropolymerization growth of PPO nanotubes inside carbon nanotubes. (B) Cyclic voltammograms for the CNM and the CN/PPO membrane (scan rate = 10 mV/s). The solution was 4 mM $K_3Fe(CN)_6$ in 0.1 M KCl.

Presumably PPO films have no surface charge although the lack of EOF is not conclusive evidence of this. It has been shown that the diffuse double layer can be absent

in charged polymers as charge compensation may actually occur in the porous matrix of the polymer.[165] It should be mentioned that the native surface charge of the carbon nanotubes could indeed be extant though the resulting electrical double layer must be completely encompassed by the PPO inner-tube. In any event, CN/PPO membranes are clearly EOF-passivated (Figure 4-4) which is further evidence that PPO nanotube growth is complete.

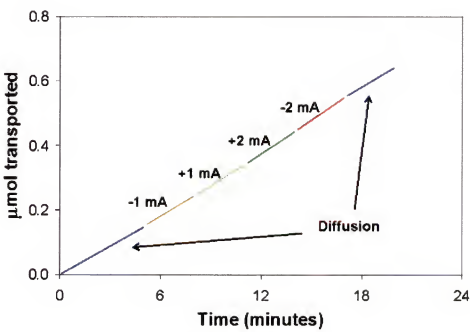

Figure 4-4. Micromoles of phenol transported vs. time at various values of applied current density across a CN/PPO membrane.

Redox-Modulated EOF in CN/PVFc Membranes

An electropolymerization method for synthesizing ultrathin films of PVFc[125] was used to coat the inner walls of the carbon nanotubes. The modification-CVs, as well as the golden color, were consistent with those reported for PVF films grown on GCEs by the same method.[125] The electrochemistry of the PVFc film within the CN/PVFc membrane can be represented as

$$PVFc \leftrightarrow PVFc^{+} + e^{-} \qquad (4\text{-}2)$$

Cyclic voltammetry using the CN/PVFc membrane as the working electrode in 0.1 M $KClO_4$ clearly shows this reversible redox reaction (Figure 4-5). The area under the voltammogram provides the moles of PVFc deposited along the nanotube walls. Ideally, we want monolayer coverage. From the inner surface area of the carbon nanotubes,[103] the moles of PVFc in the membrane, and the moles of PVFc equivalent to a monolayer,[125] we calculate that 40% of a monolayer is deposited within the nanotubes. This assumes, however, that all of the PVFc is electroactive, and this is undoubtedly not the case. These data indicate that we are close to the ideal single-monolayer coverage.

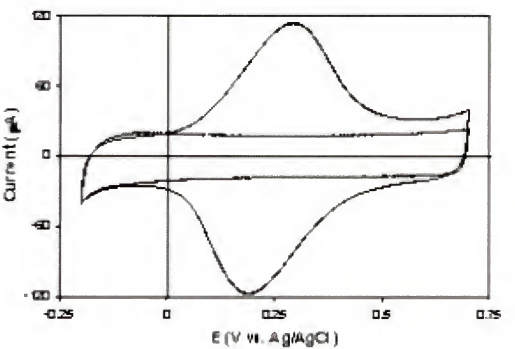

Figure 4-5. Cyclic voltammograms for the CNM and the CN/PVFc membranes. Scan rate = 10 mV s^{-1}.

We have conducted EOF experiments with CN/PVFc membranes in order to study redox modulation of EOF (Figure 4-1). EOF was measured as a function of the redox state of PVFc within the carbon nanotubes (Equation 4-2). Figure 4-6 shows plots of υ_{eo} vs. applied current density for the two extremes – +0.7 V, where all the PVFc is present

as $PVFc^+$, and -0.2 V, where all the PVFc is present as uncharged PVFc. When the polymer is in the $PVFc^+$ state the excess positive surface charge on the nanotube walls should result in a positive ζ, and this is observed experimentally (ζ = +17.2 mV).

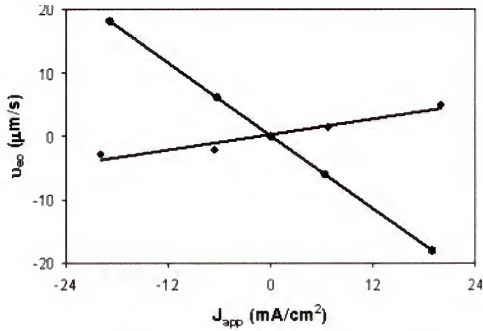

Figure 4-6. Plots of electroosmotic flow velocity vs applied current density for totally oxidized (●) and totally reduced (♦) CN/PVFc membranes.

When the polymer is reduced (PVFc form) there should be no excess surface charge, and ζ should be zero. However, a small negative ζ was obtained for the totally reduced polymer (Figure 4-6). This may be because the CNM with no PVFc could have a small negative ζ at this pH. Carboxylic acid functionalities and anionic surface adsorption are two likely explanations for this. In addition, there may be residual anionic sites on the PVFc due to air oxidation of the polymer. In any case, the negative zeta potential for the membrane when the polymer is completely reduced is fortuitous because it allows us to have EOF in one direction through the membrane when the polymer is oxidized and EOF in the opposite direction (although at a lower rate) when the polymer is totally reduced (Figure 4-6).

Finally, in addition to the two extremes – all $PVFc^+$ at +0.7 V or all PVFc at -0.2 V – the Nernst equation tells us that the ratio moles-$PVFc^+$/total-moles-PVFc can be adjusted to any value between zero and one by applying potentials intermediate between these two extremes. This should provide a way to adjust the excess positive surface charge, and thus the electroosmotic flow rate, to any value between the +0.7 V and -0.2 V limits. We have proven this point by measuring υ_{eo} after applying various potentials between these extremes to the CN/PVFc membrane. Again, the potential was applied until equilibrium had been achieved, the membrane was released from potentiostatic control, and υ_{eo} was measured. The data obtained were processed as a plot of ζ, which as Equation 4-1 shows is directly proportional to υ_{eo}, vs. potential applied to the CN/PVFc membrane (Figure 4-7).

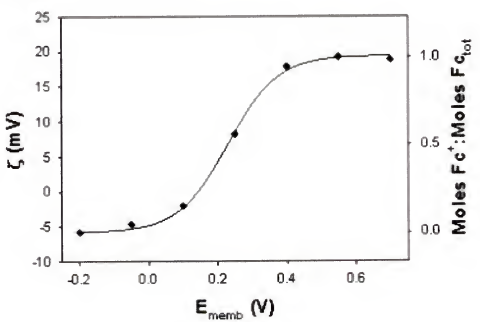

Figure 4-7. Effect of redox modulation on EOF and zeta potential of CN/PVFc membrane electrode.

Figure 4-7 shows that the zeta potential raises from its negative limit when the potential applied to the membrane is positive of 0 V and increases continuously until an

applied potential of ~+0.5 V is reached. This response is in beautiful agreement with the cyclic voltammogram (Figure 4-5) where we see that oxidation of the polymer to produce $PVFc^+$ starts at potentials positive of 0 V, and oxidation is complete when the potential reaches ~+0.5 V. Clearly, EOF has been successfully and continuously redox modulated based on the Nernstian behavior of the PVF-CNM.

It is worth noting that these PVFc films are quite robust; after an initial equilibration of ~20 cyclic voltammetry scans there is very little degradation of peak currents observed. Even after many EOF experiments, 100 or more CV scans, and aging more than a week's time, voltammetry indicates that the PVF film is largely extant and active.

Conclusions

In Chapter 3 we reported and discussed how electroosmotic flow across template-prepared carbon nanotube membranes was used to modulate molecular transport.[53] In addition, we demonstrated how electroosmotic flow could be controlled by adjusting the concentration and pH of electrolye as well as with the addition of small concentrations of surfactant.

In the work reported in this chapter we have taken advantage of the electronic conductivity of CNMs to electrochemically modify the carbon nanotube inner-walls and thus tailor the electrokinetic properties of the membrane. A cationic radical amine electrochemical derivitization method was used to attach specific anionic and cationic functional groups to the carbon nanotubes. CNMs prepared with a carboxylic functionality enhanced EOF while membranes prepared with an amino functionality reversed it.

Fully-formed, defect-free poly(phenylene oxide) nanotubes were electropolymerized within carbon nanotubes. These CN/PPO membranes were EOF-dead even while diffusive and electrophoretic modes of mass transport remained operative. EOF is detrimental for many electrophoresis-based separation techniques (e.g. isoelectric focusing) so EOF-dead membranes incorporated into electrophoresis microfluidics devices are potentially of great interest.

In addition, we have demonstrated a new approach for modulating EOF based on redox control of surface charge in poly(vinylferrocene) modified carbon nanotubes (Figure 4-1). This method should be applicable to any device or system using EOF, provided a redox polymer can be coated along the flow channel and the walls of the flow channel are electronically conductive, so that the redox state of the polymer can be changed. In some ways this approach is similar to a field-effect concept[120,121,158] in which a much larger potential (>50 V) was applied to an electronically conductive phase coated on the outside of an electronically insulating capillary or microfluidic channel. The advantage of this non-faradaic approach is that the channel itself does not need to be electronically conductive. The advantage of our approach is that much smaller voltages are needed, and the voltage must be applied for only a few seconds. Hence, in principal, redox-modulation could be implemented with only a small battery for surface charge control.

CHAPTER 5
CONCLUSIONS

Carbon nanotubes have become a burgeoning field of study in nanotechnology research since 1991.[7,12,14,15,166] Recently, the idea of using dense arrays of free-standing, open-ended carbon nanotubes as membranes has begun gaining momentum in both experimental[33,53,84] and theoretical[76-80] nanotube research. Along these lines, the underlying theme of this dissertation is tailoring the structural, physical, and chemical properties of carbon nanotube membranes in order to control and optimize the membranes transport properties.

The synthesis and structural tailoring of carbon nanotube membranes is described in depth in Chapter 2. Here, we demonstrate the key advantage of template synthesis: its inherent flexibility in tailoring nanostructures with specific characteristics. Highly-porous carbon nanotube membranes have been synthesized by CVD of disordered graphitic carbon thin films into both commercial and lab-grown AAO template membranes.[108] Using this method, carbon nanotubes are grown conforming to the shape and dimensions of the host pore. Each nanotube has an inner diameter defined by the thickness of the tube-wall and diameter of the template pore.

A number of synthesis strategies have been used to prepare carbon nanotube membranes containing nanotubes with a variety of shapes and sizes. CNMs with pore diameters >100 nm and ~20% porosities have been reproducibly synthesized for the EOF studies reported in Chapters 3 and 4. Carbon was deposited very slowly in these

membranes resulting in nanotube walls very uniform in thickness. CVD at high rates resulted in nanotubes with walls much thicker at their ends than in the middle. Bottlenecked nanotube ends we grown to diameters less than 10 nm. The bottlenecked-CNMs were asymmetric with very thin selective layers of <30 nm. Another strategy used for preparing asymmetric CNMs was to grow nanotubes in a correspondingly asymmetric template with highly branched pores. Very small nanotubes have been prepared in lab-grown AAO with uniformly 5 nm thick walls and inner diameters of ~15 nm. Finally, highly-ordered arrays of carbon nanotubes have been grown in double-anodized AAO which are near-perfect cylinders and extremely monodisperse in morphology.

Undoubtedly, the combination of such high quality alumina templates with controlled CVD will enable further tailored-growth of CNMs with a wide variety of properties and capabilities. A key challenge in membrane separations research is maximizing permeability while maintaining the required permselectivity.[59,66] The template method, with it inherent advantages in fabricating highly porous, asymmetric membranes with small and very uniform pores, is of great potential importance here.

While we have demonstrated good control of the structural properties of carbon nanotube membranes, the primary thrust of the work reported in this dissertation is towards tailoring the chemical and physicochemical properties of the membranes. In Chapters 3 and 4 we reported experiments in which we manipulated such parameters to exhibit nanofluidic control of solutions in carbon nanotube membranes. Along these lines, we flowed solutions across template-prepared carbon nanotube membranes by electroosmosis. The rate and direction of EOF was controlled by changing the magnitude and the sign of the trans-membrane current. The observed relationship between EOF and

current indicated that the as-synthesized nanotubes had substantial anionic charge. Flow in the direction of a neutral molecule, diffusing across the membrane, enhanced flux by as much as 4x. Flow in the opposite direction diminished and even halted transport of the molecule across the membrane. Electrolyte concentration was varied to compress and expand the double layer which respectively decreases and increases EOF.

The direction of electroosmotic flow was switched by varying the pH of the contacting solution. The pH-induced changes in EOF were due to titration of acidic and basic functionalities and therefore reversible. This means, for example, that returning a membrane that had been exposed to pH = 3.5 buffer, where no EOF was observed, to pH = 7.2 buffer, restored the flow. EOF was also controlled dynamically in carbon nanotube membranes with the addition of cationic surfactant to the permeation cell solutions. Due to the anionic surface charge on the nanotube wall, the surfactant self-assembled into a cationic bilayer giving the membrane a net cationic surface charge. As a result, once the surfactant-bilayer formed, EOF in the CNM reversed directions.

In work reported in Chapter 4, we took advantage of the electronic conductivity of CNMs to electrochemically modify the carbon nanotube inner-walls and control further the electroosmotic flow characteristics of the membrane. A cationic radical amine electropolymerization method[148] was used to attach specific functional groups to the carbon nanotubes. CNMs prepared with a carboxylic acid functionality enhanced EOF while membranes prepared with an amino functionality reversed it.

Fully-formed, defect-free poly(phenylene oxide) nanotubes were grown concentrically inside carbon nanotubes by electropolymerization.[124] Redox active molecules were found to be inactive once the membrane was polymerized. The CN/PPO

membranes were EOF-dead even while the diffusive and electrophoretic modes of mass transport remained operative.

Finally, we have demonstrated a new approach for modulating electroosmotic flow based on redox control of surface charge in poly(vinylferrocene) modified carbon nanotubes. When oxidized, the polymerized nanotube had positive surface charge. Electrochemically reducing the polymer converted the surface charge to negative, thus reversing EOF. This electrochemical reaction is fully reversible and can be completed in ~10 seconds. In addition, the redox-membranes follow Nernstian-based behavior allowing partial oxidation or reduction of the polymer. Therefore, EOF can be dynamically modulated to all points between the negative and positive limits.

This new method should be applicable to any device or system using EOF, provided a redox polymer can be coated along the flow channel and the walls of the flow channel are electronically conductive so that the redox state of the polymer can be changed. In some ways this approach is similar to a field-effect concept[120,121,158] in which a much larger potential (>50 V) was applied to an electronically conductive phase coated on the outside of an electronically insulating capillary or microfluidic channel. The advantage of this non-faradaic approach is that the channel itself does not need to be electronically conductive. The advantage of our approach is that much smaller voltages are needed, and the voltage must be applied for only a few seconds. Hence, in principal, redox-modulation could be implemented with only a small battery for surface charge control.

Other than theoretical studies,[77] the investigations reported here are the first examples of electroosmotic flow in carbon nanotubes or carbon membranes of any kind.

While well understood at the microscale, experimental corroboration of existing nanoscale-EOF theory is lacking.[144,145] Interestingly, the tunability and the nearly ideal pore morphologies of CNMs is potentially of great interest in providing empirical evidence in support of these same theoretical studies.[77,144,145]

One area driving interest in nanoscale electroosmotic flow is the recent incorporation of nanoporous membranes into microfluidic chips.[122,167-169] Such nano-microfluidic devices have been used, as microreactors,[168] molecular gates,[122] and for preconcentration,[169] separation,[167] and assay[168] of biomolecules. With their flexibility and tailorability, template-prepared carbon nanotube membranes could very well play a key role in this new branch of research. One possibility amongst many is the EOF-dead poly(phenyleneoxide) membrane. This type of membrane is particularly interesting, as EOF is detrimental for isoelectric focusing and at times for other electrophoresis-based separation methods as well. Incorporated into lab-on-a-chip analytical devices, template-prepared EOF membranes could open the door to a new class of membrane-based microscale analytical technologies.

LIST OF REFERENCES

(1) Davis, W. R.; Slawson, R. J.; Rigby, G. R. *Nature (London, United Kingdom)* **1953**, *171*, 756.

(2) Rodriguez, N. M. *Journal of Materials Research* **1993**, *8*, 3233-3250.

(3) Kroto, H. W.; Heath, J. R.; O'Brien, S. C.; Curl, R. F.; Smalley, R. E. *Nature (London, United Kingdom)* **1985**, *318*, 162-163.

(4) Iijima, S. *Nature (London, United Kingdom)* **1991**, *354*, 56-58.

(5) Iijima, S.; Ichihashi, T. *Nature (London, United Kingdom)* **1993**, *364*, 737.

(6) Wang, N.; Tang, Z. K.; Li, G. D.; Chen, J. S. *Nature* **2000**, *408*, 50-51.

(7) Baughman, R. H.; Zakhidov, A. A.; de Heer, W. A. *Science (Washington, DC, United States)* **2002**, *297*, 787-792.

(8) Peigney, A. *Nature Materials* **2003**, *2*, 15-16.

(9) Martin, C. R.; Kohli, P. *Nature Reviews Drug Discovery* **2003**, *2*, 29-37.

(10) Banerjee, S.; Kahn, M. G. C.; Wong, S. S. *Chemistry--A European Journal* **2003**, *9*, 1898-1908.

(11) Niyogi, S.; Hamon, M. A.; Hu, H.; Zhao, B.; Bhowmik, P.; Sen, R.; Itkis, M. E.; Haddon, R. C. *Accounts of Chemical Research* **2002**, *35*, 1105-1113.

(12) Haddon, R. C. *Accounts of Chemical Research* **2002**, *35*, 997.

(13) Tseng, G. Y.; Ellenbogen, J. C. *Science (Washington, DC, United States)* **2001**, *294*, 1293-1294.

(14) Subramoney, S. *Electrochemical Society Interface* **1999**, *8*, 34-37.

(15) Dai, H. *Surface Science* **2002**, *500*, 218-241.

(16) Dai, L.; Patil, A.; Gong, X.; Guo, Z.; Liu, L.; Liu, Y.; Zhu, D. *ChemPhysChem* **2003**, *4*, 1150-1169.

(17) Martel, R. *Nature Materials* **2002**, *1*, 203-204.

(18) Weisman, R. B. *Nature Materials* **2003**, *2*, 569-570.

(19) Dresselhaus, M. S.; Dresselhaus, G.; Eklund, P. C.; Editors *Science of Fullerenes and Carbon Nanotubes*, 1996.

(20) Kasumov, A. Y.; Deblock, R.; Kociak, M.; Reulet, B.; Bouchiat, H.; Khodos, II; Gorbatov, Y. B.; Volkov, V. T.; Journet, C.; Burghard, M. *Science* **1999**, *284*, 1508-1511.

(21) Tang, Z. K.; Zhang, L. Y.; Wang, N.; Zhang, X. X.; Wen, G. H.; Li, G. D.; Wang, J. N.; Chan, C. T.; Sheng, P. *Science* **2001**, *292*, 2462-2465.

(22) Kim, P.; Shi, L.; Majumdar, A.; McEuen, P. L. *Physical Review Letters* **2001**, *87*, 215502/215501-215502/215504.

(23) Wong, E. W.; Sheehan, P. E.; Lieber, C. M. *Science* **1997**, *277*, 1971-1975.

(24) McEuen, P. L. *Nature* **1998**, *393*, 15-+.

(25) Tans, S. J.; Verschueren, A. R. M.; Dekker, C. *Nature* **1998**, *393*, 49-52.

(26) Ouyang, M.; Huang, J. L.; Cheung, C. L.; Lieber, C. M. *Science* **2001**, *292*, 702-705.

(27) Rueckes, T.; Kim, K.; Joselevich, E.; Tseng, G. Y.; Cheung, C. L.; Lieber, C. M. *Science* **2000**, *289*, 94-97.

(28) Dillon, A. C.; Heben, M. J. *Applied Physics a-Materials Science & Processing* **2001**, *72*, 133-142.

(29) Liu, C.; Fan, Y. Y.; Liu, M.; Cong, H. T.; Cheng, H. M.; Dresselhaus, M. S. *Science* **1999**, *286*, 1127-1129.

(30) Chen, P.; Wu, X.; Lin, J.; Tan, K. L. *Science* **1999**, *285*, 91-93.

(31) Baughman, R. H.; Cui, C. X.; Zakhidov, A. A.; Iqbal, Z.; Barisci, J. N.; Spinks, G. M.; Wallace, G. G.; Mazzoldi, A.; De Rossi, D.; Rinzler, A. G.; Jaschinski, O.; Roth, S.; Kertesz, M. *Science* **1999**, *284*, 1340-1344.

(32) Che, C. L.; Miller, S. A.; Fisher, E. R.; Martin, C. R. *Analytical Chemistry* **1999**, *71*, 3187-3191.

(33) Che, G. L.; Lakshmi, B. B.; Fisher, E. R.; Martin, C. R. *Nature* **1998**, *393*, 346-349.

(34) Gao, B.; Kleinhammes, A.; Tang, X. P.; Bower, C.; Fleming, L.; Wu, Y.; Zhou, O. *Chemical Physics Letters* **1999**, *307*, 153-157.

(35) Davis, J. J.; Coleman, K. S.; Azamian, B. R.; Bagshaw, C. B.; Green, M. L. H. *Chemistry--A European Journal* **2003**, *9*, 3732-3739.

(36) Azamian, B. R.; Davis, J. J.; Coleman, K. S.; Bagshaw, C. B.; Green, M. L. H. *Journal of the American Chemical Society* **2002**, *124*, 12664-12665.

(37) Kong, J.; Franklin, N. R.; Zhou, C.; Chapline, M. G.; Peng, S.; Cho, K.; Dai, H. *Science* **2000**, *287*, 622-625.

(38) Wong, S. S.; Joselevich, E.; Woolley, A. T.; Cheung, C. L.; Lieber, C. M. *Nature* **1998**, *394*, 52-55.

(39) de Heer, W. A. *Nature Materials* **2002**, *1*, 153-154.

(40) Fan, S. S.; Chapline, M. G.; Franklin, N. R.; Tombler, T. W.; Cassell, A. M.; Dai, H. J. *Science* **1999**, *283*, 512-514.

(41) Dai, H. *Accounts of Chemical Research* **2002**, *35*, 1035-1044.

(42) Ding, R. G.; Lu, G. Q.; Yan, Z. F.; Wilson, M. A. *Journal of Nanoscience and Nanotechnology* **2001**, *1*, 7-29.

(43) Kong, J. S., Hyongsok T. Cassell, Alan M. Quate, Calvin F. Dai, Hongjie In *Nature*; Nature Publishing Group, 1998; Vol. 395, p 878.

(44) Kong, J.; Cassell, A. M.; Dai, H. J. *Chemical Physics Letters* **1998**, *292*, 567-574.

(45) Teo, K. B. K.; Chhowalla, M.; Amaratunga, G. A. J.; Milne, W. I.; Hasko, D. G.; Pirio, G.; Legagneux, P.; Wyczisk, F.; Pribat, D. *Applied Physics Letters* **2001**, *79*, 1534-1536.

(46) Franklin, N. R.; Dai, H. J. *Advanced Materials* **2000**, *12*, 890-894.

(47) Cassell, A. M.; Franklin, N. R.; Tombler, T. W.; Chan, E. M.; Han, J.; Dai, H. J. *Journal of the American Chemical Society* **1999**, *121*, 7975-7976.

(48) Zhang, Y. G.; Chang, A. L.; Cao, J.; Wang, Q.; Kim, W.; Li, Y. M.; Morris, N.; Yenilmez, E.; Kong, J.; Dai, H. J. *Applied Physics Letters* **2001**, *79*, 3155-3157.

(49) Hulteen, J. C.; Martin, C. R. *Journal of Materials Chemistry* **1997**, *7*, 1075-1087.

(50) Martin, C. R. *Science* **1994**, *266*, 1961-1966.

(51) Martin, C. R.; Mitchell, D. T. *Analytical Chemistry* **1998**, *70*, 322A-327A.

(52) Kyotani, T.; Tsai, L. F.; Tomita, A. *Chemistry of Materials* **1996**, *8*, 2109-2113.

(53) Miller, S. A.; Young, V. Y.; Martin, C. R. *Journal of the American Chemical Society* **2001**, *123*, 12335-12342.

(54) Miller, S. A.; Martin, C. R. In *Encyclopedia of Nanoscience and Nanotechnology*; Schwarz, J. A., Contescu, C., K., P., Eds.; Marcel Dekker, Inc.: New York, In Press.

(55) Che, G.; Lakshmi, B. B.; Martin, C. R.; Fisher, E. R.; Ruoff, R. S. *Chemistry of Materials* **1998**, *10*, 260-267.

(56) Kyotani, T.; Tsai, L. F.; Tomita, A. *Chemical Communications* **1997**, 701-702.

(57) Papadopoulos, J. L. In *Nature*; Nature Publishing Group, 1999; Vol. 402, p 253.

(58) Patrick, J. W., Ed. *Porosity in carbons: characterization and applications*; Halsted Press: New York, 1995.

(59) Ismail, A. F.; David, L. I. B. *Journal of Membrane Science* **2001**, *193*, 1-18.

(60) Koresh, J. E.; Sofer, A. *Separation Science and Technology* **1983**, *18*, 723-734.

(61) Rao, M. B.; Sircar, S. *Journal of Membrane Science* **1993**, *85*, 253-264.

(62) Shusen, W.; Meiyun, Z.; Zhizhong, W. *Journal of Membrane Science* **1996**, *109*, 267-270.

(63) Jones, C. W.; Koros, W. J. *Carbon* **1994**, *32*, 1419-1425.

(64) Hayashi, J.; Mizuta, H.; Yamamoto, M.; Kusakabe, K.; Morooka, S. *J. Membr. Sci.* **1997**, *124*, 243.

(65) Soffer, A.; Azariah, M.; Amar, A.; Cohen, H.; Golub, D.; Saguee, S.; Tobias, H.; Rotem Industries Ltd.: U.S., 1997.

(66) Koros, W. *Chemical Engineering Progress* **1995**, *91*, 68.

(67) Geiszler, V. C. K., W.J. *Ind. Eng. Chem. Res.* **1996**, *35*, 2999.

(68) Koresh, J.; Soffer, A. *Journal of Electroanalytical Chemistry and Interfacial Electrochemistry* **1983**, *147*, 223-234.

(69) Eliad, L.; Salitra, G.; Soffer, A.; Aurbach, D. *Journal of Physical Chemistry B* **2001**, *105*, 6880-6887.

(70) Eliad, L.; Salitra, G.; Soffer, A.; Aurbach, D. *Journal of Physical Chemistry B* **2002**, *106*, 10128-10134.

(71) Lakshmi, B. B.; Martin, C. R. *Nature* **1997**, *388*, 758-760.

(72) Zhou, D.; Too, C. O.; Wallace, G. G.; Hodges, A. M.; Mau, A. W. H. *Reactive & Functional Polymers* **2000**, *45*, 217-226.

(73) Lee, S. B.; Martin, C. R. *Journal of the American Chemical Society* **2002**, *124*, 11850-11851.

(74) Nishizawa, M.; Menon, V. P.; Martin, C. R. *Science* **1995**, *268*, 700-702.

(75) Baum, R. M. *Chemical & Engineering News* **1997**, *75*, 39-41.

(76) Joseph, S.; Mashl, R. J.; Jakobsson, E.; Aluru, N. R. *Nano Letters* **2003**, *3*, 1399-1403.

(77) Qiao, R.; Aluru, N. R. *Nano Letters* **2003**, *3*, 1013-1017.

(78) Skoulidas, A. I.; Ackerman, D. M.; Johnson, J. K.; Sholl, D. S. *Physical Review Letters* **2002**, *89*, 185901/185901-185901/185904.

(79) Kalra, A.; Garde, S.; Hummer, G. *Proceedings of the National Academy of Sciences of the United States of America* **2003**, *100*, 10175-10180.

(80) Zhu, F.; Schulten, K. *Biophys. J.* **2003**, *85*, 236-244.

(81) Ren, Z. F.; Huang, Z. P.; Xu, J. W.; Wang, J. H.; Bush, P.; Siegal, M. P.; Provencio, P. N. *Science* **1998**, *282*, 1105-1107.

(82) Li, W. Z.; Xie, S. S.; Qian, L. X.; Chang, B. H.; Zou, B. S.; Zhou, W. Y.; Zhao, R. A.; Wang, G. *Science* **1996**, *274*, 1701-1703.

(83) Schlittler, R. R.; Seo, J. W.; Gimzewski, J. K.; Durkan, C.; Saifullah, M. S. M.; Welland, M. E. *Science* **2001**, *292*, 1136-1139.

(84) Sun, L.; Crooks, R. M. *Journal of the American Chemical Society* **2000**, *122*, 12340-12345.

(85) Che, G. L.; Lakshmi, B. B.; Martin, C. R.; Fisher, E. R. *Langmuir* **1999**, *15*, 750-758.

(86) Penner, R. M.; Martin, C. R. *Analytical Chemistry* **1987**, *59*, 2625-2630.

(87) Cheng, I. F.; Martin, C. R. *Analytical Chemistry* **1988**, *60*, 2163-2165.

(88) Possin, G. E. *Review of Scientific Instruments* **1970**, *41*, 772-&.

(89) Huczko, A. *Applied Physics A: Materials Science & Processing* **2000**, *70*, 365-376.

(90) Martin, C. R. *Accounts of Chemical Research* **1995**, *28*, 61-68.

(91) Martin, C. R. *Chemistry of Materials* **1996**, *8*, 1739-1746.

(92) Wirtz, M.; Miller, S. A.; Martin, C. R. *International Journal of Nanoscience* **2002**, *1*, 255-268.

(93) Liang, Z.; Susha, A. S.; Yu, A.; Caruso, F. *Advanced Materials (Weinheim, Germany)* **2003**, *15*, 1849-1853.

(94) Patrissi, C. J.; Martin, C. R. *Journal of the Electrochemical Society* **1999**, *146*, 3176-3180.

(95) Jirage, K. B.; Hulteen, J. C.; Martin, C. R. *Science* **1997**, *278*, 655.

(96) Menon, V. P.; Martin, C. R. *Analytical Chemistry* **1995**, *67*, 1920-1928.

(97) Harrell, C. C.; Lee, S. B.; Martin, C. R. *Analytical Chemistry* **1993**, *75*, 6861-6867.

(98) Siwy, Z.; Gu, Y.; Spohr, H. A.; Baur, D.; Wolf-Reber, A.; Spohr, R.; Apel, P.; Korchev, Y. E. *Europhysics Letters* **2002**, *60*, 349-355.

(99) Fleischer, R. L.; Price, P. B.; Walker, R. M. *Nuclear Tracks in Solids*; Univ. of California Press: Berkeley, CA, 1975.

(100) Wirtz, M.; Yu, S.; Martin, C. R. *Analyst (Cambridge, United Kingdom)* **2002**, *127*, 871-879.

(101) Kobayashi, Y.; Martin, C. R. *Analytical Chemistry* **1999**, *71*, 3665-3672.

(102) Tsai, S. H.; Chao, C. W.; Lee, C. L.; Liu, X. W.; Lin, I. N.; Shih, H. C. *Electrochemical and Solid-State Letters* **1999**, *2*, 247.

(103) Crawford, G. P.; Steele, L. M.; Ondriscrawford, R.; Iannacchione, G. S.; Yeager, C. J.; Doane, J. W.; Finotello, D. *Journal of Chemical Physics* **1992**, *96*, 7788-7796.

(104) Furneaux, R. C.; Rigby, W. R.; Davidson, A. P. *Nature* **1989**, *337*, 1989.

(105) Foss Jr., C. A.; Hornyak, G. L.; Stockert, J. A.; Martin, C. R. *Journal of Physical Chemistry* **1994**, *98*, 2963.

(106) Masuda, H.; Fukuda, K. *Science* **1995**, *268*, 1466-1468.

(107) Li, F.; Zhang, L.; Metzger, R. M. *Chemistry of Materials* **1998**, *10*, 2470.

(108) Trofin, L. D.; Mitchell, D. T.; Martin, C. R. *Unpublished work.*

(109) Jessensky, O.; Muller, F.; Gosele, U. *Journal of the Electrochemical Society* **1998**, *145*, 3735.

(110) Masuda, H.; Yamada, H.; Satoh, M.; Asoh, H.; Nakao, M.; Tamamura, T. *Applied Physics Letters* **1997**, *71*, 2770-2772.

(111) Kemery, P. J.; Steehler, J. K.; Bohn, P. W. *Langmuir* **1998**, *14*, 2884-2889.

(112) Bath, B. D.; Lee, R. D.; White, H. S.; Scott, E. R. *Analytical Chemistry* **1998**, *70*, 1047-1058.

(113) Bath, B. D.; White, H. S.; Scott, E. R. *Analytical Chemistry* **2000**, *72*, 433-442.

(114) Kuo, T. C.; Sloan, L. A.; Sweedler, J. V.; Bohn, P. W. *Langmuir* **2001**, *17*, 6298-6303.

(115) Polson, N. A.; Hayes, M. A. *Analytical Chemistry* **2001**, *73*, 312A-319A.

(116) Ghatak-Roy, A. R.; Martin, C. R. *Analytical Chemistry* **1986**, *58*, 1574.

(117) Deinhammer, R. S.; Shimazu, K.; Porter, M. D. *Analytical Chemistry* **1991**, *63*, 1889.

(118) Deinhammer, R. S.; Ting, E.; Porter, M. C. *Analytical Chemistry* **1995**, *67*, 237.

(119) Lam, P.; Kumar, K.; Wnek, G. E.; Przybycien, T. M. *Analytical Chemistry* **1999**, *71*, 4272.

(120) Lee, C. S.; Blanchard, W. C.; Wu, C. *Analytical Chemistry* **1990**, *62*, 1550.

(121) Schasfoort, R. B. M.; Schlautmann, S.; Hendrikse, L.; van den Berg, A. *Science* **1999**, *286*, 942-945.

(122) Kuo, T. C.; Cannon, D. M.; Chen, Y. N.; Tulock, J. J.; Shannon, M. A.; Sweedler, J. V.; Bohn, P. W. *Analytical Chemistry* **2003**, *75*, 1861-1867.

(123) Cannon, D. M.; Kuo, T. C.; Bohn, P. W.; Sweedler, J. V. *Analytical Chemistry* **2003**, *75*, 2224-2230.

(124) Oyama, N.; Ohsaka, T.; Ohnuki, Y.; Suzuki, T. *Journal of the Electrochemical Society* **1987**, *134*, 3068-3073.

(125) Ju, H. X.; Leech, D. *Journal of the Chemical Society-Faraday Transactions* **1997**, *93*, 1371-1375.

(126) Jirage, K. B.; Hulteen, J. C.; Martin, C. R. *Analytical Chemistry* **1999**, *71*, 4913-4918.

(127) Kang, M. S.; Martin, C. R. *Langmuir* **2001**, *17*, 2753-2759.

(128) Hornyak, G. L.; Patrissi, C. J.; Martin, C. R. *Journal of Physical Chemistry B* **1997**, *101*, 1548-1555.

(129) Morosanu, C. E. *Thin Films by Chemical Vapour Deposition*; Elsevier: Amsterdam, 1990; Vol. 7.

(130) Joo, S. H.; Choi, S. J.; Oh, I.; Kwak, J.; Liu, Z.; Terasaki, O.; Ryoo, R. *Nature* **2001**, *412*, 169-172.

(131) Deheer, W. A.; Chatelain, A.; Ugarte, D. *Science* **1995**, *270*, 1179-1180.

(132) Lucy, C. A.; Underhill, R. S. *Analytical Chemistry* **1996**, *68*, 300-305.

(133) Panzer, R. E.; Elving, P. J. *Electrochimica Acta* **1975**, *20*, 635-647.

(134) Bismarck, A.; Springer, J. *Colloids and Surfaces a-Physicochemical and Engineering Aspects* **1999**, *159*, 331-339.

(135) Garcia, A. B.; Cuesta, A.; MontesMoran, M. A.; MartinezAlonso, A.; Tascon, J. M. D. *Journal of Colloid and Interface Science* **1997**, *192*, 363-367.

(136) Powell, C. J.; Jablonski, A.; Tilinin, I. S.; Tanuma, S.; Penn, D. R. *Journal of Electron Spectroscopy and Related Phenomena* **1999**, *99*, 1-15.

(137) Yaws, C. L. *Handbook of Transport Property Data*, 1995.

(138) Ramm, M.; Ata, M.; Brzezinka, K. W.; Gross, T.; Unger, W. *Thin Solid Films* **1999**, *354*, 106-110.

(139) Beamson, G.; Briggs, D.; Wiley, Chichester: England, 1992, pp 82-179.

(140) Srinivasan, V.; Higuchi, W. I. *International Journal of Pharmaceutics* **1990**, *60*, 133-138.

(141) Renkin, E. M. *Journal of General Physiology* **1954**, *38*, 225-243.

(142) Probstein, R. F.; Buttersworth: Stoneham, MA, 1989, pp 185-198.

(143) Weast, R. C.; Astle, M. J.; Beyer, W. H., Eds. *CRC Handbook of Chemistry and Physics*; 66th ed.; CRC Press, Inc.: Boca Raton, FL, 1985.

(144) Rice, C. L.; Whitehead, R. *Journal of Physical Chemistry* **1965**, *69*, 4024.

(145) Levine, S.; Marriott, J. R.; Neale, G.; Epstein, N. *Journal of Colloid and Interface Science* **1975**, *52*, 136-149.

(146) Jimbo, T.; Tanioka, A.; Minoura, N. *Langmuir* **1998**, *14*, 7112-7118.

(147) Leon y Leon, C. A.; Solar, J. M.; Calemma, V.; Radovic, L. R. *Carbon* **1992**, *30*, 797-811.

(148) Liu, J. Y.; Cheng, L.; Li, B. F.; Dong, S. J. *Langmuir* **2000**, *16*, 7471-7476.

(149) Saby, C.; Ortiz, B.; Champagne, G. Y.; Belanger, D. *Langmuir* **1997**, *13*, 6805-6813.

(150) Cheng, I. F.; Whiteley, L. D.; Martin, C. R. *Analytical Chemistry* **1989**, *61*, 762-766.

(151) Tavares, M. F. M.; Colombara, R.; Massaro, S. *Journal of Chromatography A* **1997**, *772*, 171-178.

(152) Burns, D. B.; Zydney, A. L. *Journal of Membrane Science* **2000**, *172*, 39-48.

(153) Martin, C. R.; Nishizawa, M.; Jirage, K.; Kang, M. S.; Lee, S. B. *Advanced Materials* **2001**, *13*, 1351-1362.

(154) Cepak, V. M.; Hulteen, J. C.; Che, G. L.; Jirage, K. B.; Lakshmi, B. B.; Fisher, E. R.; Martin, C. R.; Yoneyama, H. *Chemistry of Materials* **1997**, *9*, 1065-&.

(155) Miller, S. A.; Martin, C. R. *Journal of Electroanalytical Chemistry* **2002**, *522*, 66-69.

(156) Liu, Y.; Fanguy, J. C.; Bledsoe, J. M.; Henry, C. S. *Analytical Chemistry* **2000**, *72*, 5939-5944.

(157) Moorthy, J.; Khoury, C.; Moore, J. S.; Beebe, D. J. *Sensors and Actuators B-Chemical* **2001**, *75*, 223-229.

(158) Hayes, M. A.; Ewing, A. G. *Analytical Chemistry* **1992**, *64*, 512.

(159) Horvath, J.; Dolnik, V. *Electrophoresis* **2001**, *22*, 644-655.

(160) Righetti, P. G.; Gelfi, C.; Verzola, B.; Castelletti, L. *Electrophoresis* **2001**, *22*, 603-611.

(161) Barbier, B.; Pinson, J.; Desarmot, G.; Sanchez, M. *Journal of the Electrochemical Society* **1990**, *137*, 1757-1764.

(162) Deinhammer, R. S.; Ho, M.; Anderegg, J. W.; Porter, M. D. *Langmuir* **1994**, *10*, 1306-1313.

(163) Ohsaka, T.; Hirokawa, T.; Miyamoto, H.; Oyama, N. *Analytical Chemistry* **1987**, *59*, 1758-1761.

(164) Abruna, H. D.; Denisevich, P.; Umana, M.; Meyer, T. J.; Murray, R. W. *Journal of the American Chemical Society* **1981**, *103*, 1-5.

(165) Wang, J.; Bard, A. J. *Journal of the American Chemical Society* **2001**, *123*, 498-499.

(166) Baughman, R. H. *Science* **2000**, *290*, 1310-1311.

(167) Wang, P.-C.; DeVoe, D. L.; Lee, C. S. *Electrophoresis* **2001**, *22*, 3857-3867.

(168) Ismagilov, R. F.; Ng, J. M. K.; Kenis, P. J. A.; Whitesides, G. M. *Analytical Chemistry* **2001**, *73*, 5207-5213.

(169) Zhang, Y.; Timperman Aaron, T. *ANALYST* **2003**, *128*, 537-542.

BIOGRAPHICAL SKETCH

Scott A. Miller was born in Seattle, Washington to Allan and Barbara Miller. Soon after, the family moved to Richland, Washington where Scott grew up with his older brother Burnie and younger sister Brenda. Watching his father's career as a Ph.D. chemist develop from research scientist to entrepreneur Scott began developing his own interests in science and technology. Scott graduated from high school in Richland while working for a DOE contractor at the Hanford Nuclear Reservation. He attended college at Graceland College in Lamoni, Iowa where he studied Chemistry. Upon graduation, Scott worked for Analytical Technologies, Inc. in Fort Collins, Colorado before returning to Richland to work for Chemchek Instruments, Inc. Eventually, Scott renewed his study of Chemistry, attending Colorado State University and University of Florida and working for Professor Charles Martin. In his free time, Scott plays competitive "ultimate" and enjoys his black lab Lennon, backpacking, and skiing.

I certify that I have read this study and that in my opinion it conforms to acceptable standards of scholarly presentation and is fully adequate, in scope and quality, as a dissertation for the degree of Doctor of Philosophy.

Charles R. Martin, Chairman
Professor of Chemistry and Anesthesiology

I certify that I have read this study and that in my opinion it conforms to acceptable standards of scholarly presentation and is fully adequate, in scope and quality, as a dissertation for the degree of Doctor of Philosophy.

Vaneica Y. Young
Associate Professor of Chemistry

I certify that I have read this study and that in my opinion it conforms to acceptable standards of scholarly presentation and is fully adequate, in scope and quality, as a dissertation for the degree of Doctor of Philosophy.

Weihong Tan
Professor of Chemistry

I certify that I have read this study and that in my opinion it conforms to acceptable standards of scholarly presentation and is fully adequate, in scope and quality, as a dissertation for the degree of Doctor of Philosophy.

Lisa A. McElwee-White
Professor of Chemistry

I certify that I have read this study and that in my opinion it conforms to acceptable standards of scholarly presentation and is fully adequate, in scope and quality, as a dissertation for the degree of Doctor of Philosophy.

Eric Wachsman
Professor of Materials Science and Engineering

This dissertation was submitted to the Graduate Faculty of the Department of English in the College of Liberal Arts and Sciences and to the Graduate School and was accepted as partial fulfillment of the requirements for the degree of Doctor of Philosophy.

May 2004

Dean, Graduate School